

EPSC2018

OPS1 abstracts

Modelling of seasonal lake level fluctuations of Titan's seas/lakes

Tetsuya Tokano (1) and Ralph D. Lorenz (2)

(1) Institut für Geophysik und Meteorologie, Universität zu Köln, Germany (tokano@geo.uni-koeln.de), (2) Johns Hopkins University Applied Physics Laboratory, Laurel, MD, USA.

Abstract

Seasonal variations in the lake level of Titan's seas and lakes are predicted by a 3-dimensional ocean circulation model under a couple of assumptions and with meteorological input data from a global climate model. The simulations are meant to help understand possible shoreline changes of Titan's lakes observed by Cassini and to constrain the nature of hydrology of these lakes. The magnitude and timing of lake level fluctuations depend on many factors such as precipitation, size of lakes and their catchment area, geographic latitude or lake composition. Ontario Lacus potentially experiences larger lake level fluctuations than the northern seas because of its larger relative catchment area, but they are compromised by the smaller methane mole fraction and smaller annual precipitation compared to the northern seas.

1. Introduction

Titan's polar region contains numerous hydrocarbon seas/lakes, but their distribution exhibits a hemispheric dichotomy in that most lakes are concentrated near the north pole [1]. Cassini observed possible temporal changes of shorelines of one of the lakes (Ontario Lacus) [2,3]. However, it is uncertain whether the observed temporal changes, if real, represent a seasonal effect or part of a longer-term variation, e.g. externally forced by orbital parameter variations (Croll-Milankovitch cycle) [1].

The current study aims at numerically predicting seasonal lake level fluctuations of different lakes in an effort to better understand the observed possible changes of the lake appearance [2,3] and assess the lake formation mechanism. Fluctuating sea/lake levels can also profoundly influence the character of shoreline erosion (by spreading wave action over a wider area) and fluvial erosion, by changing the base level for river flow. Similarly, the morphology of

fluvial deposition structures (e.g. deltas) depends on sea level fluctuations, whether due to tides or seasonal filling/drainage.

2. Methods

Seasonal lake level changes are numerically predicted by keeping track of all methane sources (precipitation, runoff) and sinks (evaporation) in a 3-dimensional ocean model. The observed lake distribution and assumed bathymetry are explicitly taken into account for the sake of precise predictions of lake volume changes. Lake evaporation is calculated as a function of lake surface temperature, composition and wind speed. The model takes the form of a 3-dimensional ocean circulation model [4], which simulates wind-driven and density-driven circulation. Input data (surface insolation, precipitation, surface wind) as functions of season and latitude are provided by a global climate model (updated version of [5]). The runoff from the catchment area [6,7] is taken into account under different assumptions (no runoff, quick surface runoff, slow groundwater seepage). The bathymetry map of the northern seas/lakes is adopted from [8] but with some updates. The bathymetry map of Ontario Lacus in the south is constructed analogously. By default, the seas/lakes have the compositions constrained by Cassini radar [9,10], yet alternative compositions are also tested.

3. Preliminary results

Ontario Lacus can potentially undergo larger seasonal lake level fluctuations than the northern seas given the extraordinarily large catchment area compared to the lake size [7]. Summer precipitation can raise the lake level by a few metres. On the other hand, evaporation is generally slower because of the low methane mole fraction in this lake. However, if mixing is weak, a methane-rich surface layer may persist and permit more rapid evaporation than if the

methane were mixed down into the less volatile ethane-rich depths.

Seasonal lake level fluctuations are generally more moderate in the northern seas because the catchment areas are not orders of magnitude larger than the seas themselves [6]. Evaporation is faster than in Ontario Lacus because of the higher methane mole fraction. Depending on the precipitation rate and nature of the runoff, the lake level can undergo a repeatable annual cycle or a gradual year-to-year increase or decrease.

Acknowledgements

TT is supported by DFG Grant TO 269/4-2, RL by NASA OPR Grant NNX13AK97G.

References

- [1] Aharonson, O., et al.: An asymmetric distribution of lakes on Titan as a possible consequence of orbital forcing, *Nat. Geosci.*, Vol. 2, pp. 851-854, 2009.
- [2] Hayes, A. G., et al.: Transient surface liquid in Titan's polar regions from Cassini, *Icarus*, Vol. 211, pp. 655-671, 2011.
- [3] Turtle, E. P., et al.: Shoreline retreat at Titan's Ontario Lacus and Arrakis Planitia from Cassini Imaging Science Subsystem observations, *Icarus*, Vol. 212, pp. 957-959, 2011.
- [4] Tokano, T., and Lorenz, R. D.: Sun-stirred Kraken Mare: Circulation in Titan's seas induced by solar heating and methane precipitation, *Icarus*, Vol. 270, pp. 67-84, 2016.
- [5] Tokano, T.: Impact of seas/lakes on polar meteorology of Titan: Simulation by a coupled GCM-sea model, *Icarus*, Vol. 204, pp. 619-636, 2009.
- [6] Lorenz, R. D.: The flushing of Ligeia: Composition variations across Titan's seas in a simple hydrological model, *Geophys. Res. Lett.*, Vol. 41, doi:10.1002/2014GL061133, 2014.
- [7] Dhingra, R. D., et al.: Large catchment area recharges Titan's Ontario Lacus, *Icarus*, Vol. 299, pp. 331-338, 2018.
- [8] Lorenz, R. D., et al.: A radar map of Titan seas: Tidal dissipation and ocean mixing through the throat of Kraken, *Icarus*, Vol. 237, pp. 9-15, 2014.

[9] Mastrogiuseppe, M. et al.: The bathymetry of a Titan sea, *Geophys. Res. Lett.*, Vol. 41, doi:10.1002/2013GL058618, 2014.

[10] Mastrogiuseppe, M., et al.: Bathymetry and composition of Titan's Ontario lacus derived from Monte Carlo-based waveform inversion of Cassini RADAR altimetry data, *Icarus*, Vol. 300, pp. 203-209, 2018.

Saturn atmospheric dynamics after Cassini from ground-based observations in the visible punctuated by HST/OPAL yearly observations

R. Hueso (1), A. Sánchez-Lavega(1), A.A. Simon(2), M.H. Wong(3), M. Delcroix(4), J.F. Rojas(1), F. Colas(5), J.M. Gómez(6), T. Barry(7).
 (1) UPV/EHU, Spain, (2) NASA GSFC, USA, (3) UC Berkeley, USA, (4) Societé Astronomique de France, Paris, France, (5) IMCCE, Observatoire de Paris, Paris, France (6) Fundacio Observatorio Esteve Duran, Barcelona, Spain, (7) Broken Hill Observatory, New South Wales, Australia (ricardo.hueso@ehu.es)

Abstract

The Cassini Mission observed the Saturn system over half a Saturn year obtaining detailed information of the atmosphere of the planet. Saturn's seasons produce changes in the Polar Regions and the bands of the planet. Like Jupiter, Saturn is a dynamic planet with variable phenomena that cannot be predicted. Winds have been observed to vary in the equatorial latitudes and small and large-scale storms and other non-convective perturbations have also been observed. We explore the capability to study atmosphere dynamics of Saturn with new data obtained from ground-based telescopes including amateur observations, observations at the 1-m planetary telescope at the Pic du Midi observatory and our own observations with the PlanetCam instrument on the 2.2m telescope at the Calar Alto observatory in Spain. Saturn images will be acquired by the HST as part of its OPAL program in June this year. The comparison of HST data with ground-based images obtained several times per week permit to study the history of several atmospheric features including a long-lived polar perturbation (months) and a very long-lived equatorial storm (years). The drift rates of some of these features and their lifetimes allow identification of the features in Cassini ISS images obtained in 2016-2017.

1. Amateur observations of Saturn

Amateur observations of Solar System planets are contributing to a time-resolved vision of the atmosphere dynamics of Jupiter and Saturn. For Saturn current observations show a display of activity not present at the time of the Cassini mission. The main new feature is a polar disturbance at 60°N (see

Figure 1) and an equatorial bright feature active at least since 2014 [1]. Analysis of ground-based data shows that several features can be identified repeatedly (see Figure 2).



Figure 1: Saturn image obtained by C. Go (Philippines) in April 2017.

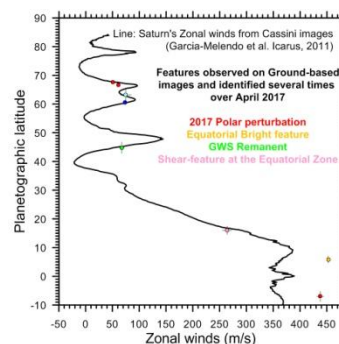


Figure 2: Saturn zonal winds from Cassini ISS compared with tracking of cloud features over April 2017 from amateur images far from opposition.

2. Ground-based Pic du Midi and PlanetCam data

Since 2013 we perform yearly observations of Saturn with the PlanetCam instrument on the 2.2 m

telescope at Calar Alto Observatory. We also analyze images obtained at the 1-m planetary telescope at the Pic du Midi Observatory. Typically, 1-3 campaigns with Saturn data are possible in each telescope each year. Figures 3-4 show examples of past observations but new observations are planned this year and we will present their analysis in comparison with the time-resolved amateur data (several observations per week).

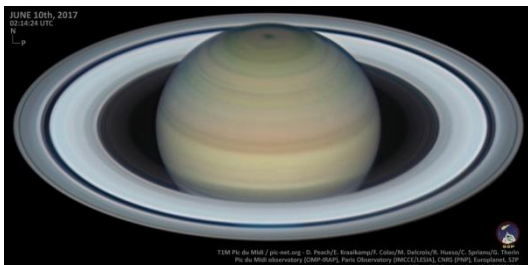


Figure 3: Saturn in the visible observed at the Pic du Midi with the 1.05m planetary telescope in July 2017 at a low elevation of the planet but with good seeing. This image was part of the Pic-Net collaboration and was processed by D. Peach.

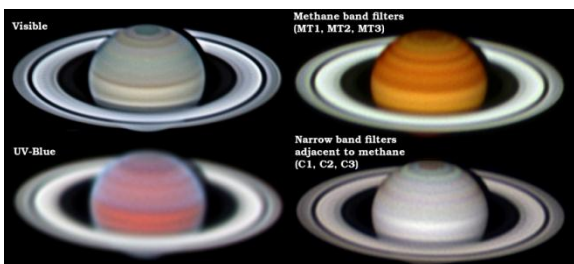


Figure 4: Multi-wavelength images in the visible range (0.4-1.0 μm) with PlanetCam UPV/EHU. The dual camera allows to observe simultaneously also in the 1.0-1.7 microns range (not shown). PlanetCam images can be absolutely calibrated studying photometric variations of the bands in the planet.

3. HST/OPAL

The Outer Planets Atmospheres Legacy HST program observes the giant planets once per year [3]. First observations of Saturn from this program will be obtained on June 6 2017. Saturn was observed by HST on 2015 due to the onset of a polar perturbation [1,2] and observations in 2015 show a variety of atmospheric features at other latitudes that are identified in the ground-based amateur record over the last 4 years. We will show the correspondence of

ground-based time-resolved observations and HST features observed close to Saturn's opposition.



Figure 5: Saturn observed by the HST in 2015 showing a variety of atmospheric features and disturbances [1, 2]. New HST observations will be acquired in June 2018 as part of the OPAL program.

4. Summary and Conclusions

The combined analysis of temporally resolved ground-based and HST images of Saturn in the visible range show changes in the planet and new meteorological activity not observed at the time of the Cassini mission. We will present this activity and the comparison of the different datasets.

Acknowledgements

We are very grateful to the ensemble of amateur astronomers that contribute their observations to open databases like PVOL and ALPO-Japan and that regularly produce high-quality observations. We are particularly grateful to D. Peach, T. Olivetti, C. Go, C. Foster, P. Miles and A. Wesley.

References

- [1] Sánchez-Lavega, A., et al. An enduring rapidly moving storm as a guide to Saturn's Equatorial jet's complex structure, *Nature Comm*, 7, 13262, 2016.
- [2] del Río-Gaztelurrutia, T., et al., A planetary scale disturbance in a long-living three vortex coupled system in Saturn's atmosphere, *Icarus*, 302, 499-513, 2018.
- [3] Simon, A., et al.: First results from OPAL program: Jupiter in 2015, *ApJ*, 812, 55, 8 pp., 2015.

Some problems in interpretation of the New Horizons observations of Pluto's atmosphere

Vladimir A Krasnopolsky

Moscow Institute of Physics and Technology, Moscow, Russia (vlad.krasn@verizon.net)

Please make sure that your pdf conversion results in a document with a page size of 237 x 180 mm!

Abstract

Here I briefly discuss (1) restrictions to LTE in the rotational lines of H₂O and HCN and their effect on thermal balance of the atmosphere, (2) comparison of the model by Zhang et al. with Titan's data, (3) contradictions in the H₂O influx from ablation of the interplanetary dust, (4) great differences between the haze observations and the model, and (5) some inconsistencies in the photochemical models.

1. Introduction

The radio and solar UV occultations and haze images at various phase angles observed during the New Horizons (NH) flyby of the Pluto system provide valuable information on the properties of Pluto's atmosphere, its thermal structure and chemical composition. Here we will briefly discuss some problems, difficulties, and inconsistencies that appear in existing published interpretation of the observational data.

2. Thermal balance

Pluto's upper atmosphere appears to be a cryosphere at $T \approx 70$ K [1] instead of the expected hydrodynamically escaping thermosphere. Strobel and Zhu [2] explained the observed cryosphere using the LTE cooling by H₂O and HCN rotational lines up to 1200 km (Fig. 1). However, the LTE conditions for rotational lines become invalid for $A \geq kn$. Here A is the transition probability, $k \approx 10^{-11} T^{1/2} \text{ cm}^3 \text{ s}^{-1}$ is the collisional rate coefficient, and n is the atmospheric number density. This means that the assumption of LTE becomes invalid for H₂O and HCN above 700 and 820 km, respectively, and significantly affects the model results above 700 km (Fig. 1).

Zhang et al. [3] proved that the observed haze is more effective in heating and cooling of the atmosphere than the atmospheric gases. They extrapolated the haze attenuation measured by the

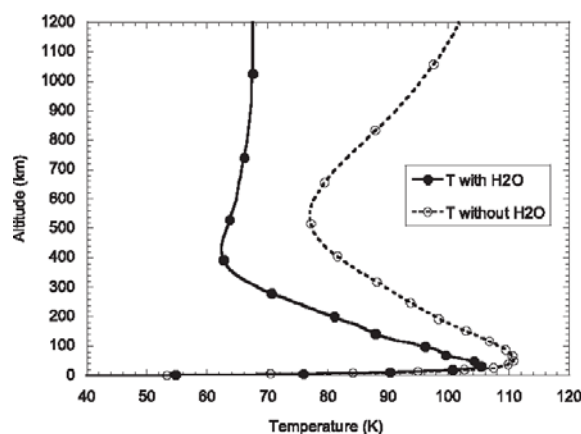


Fig. 1. Temperature profiles with and without H₂O cooling. From Strobel and Zhu [2].

NH UV solar occultations from 350 to 700 km and adopted the particle radius of 10 nm for these altitudes. The haze heats the atmosphere by absorption of the solar light in the visible and cools by thermal radiation at 10-300 μm . The authors succeeded to fit the observed temperatures if the haze absorption coefficient is smaller by a factor of 4 in the visible and greater by a factor of 2.5 in the thermal infrared than that measured by Khare et al. [4] in their laboratory study. Both changes are opposite to those observed by the Cassini VIMS and CIRS on Titan [5]. However, absorption coefficient of the very small particles above 350 km on Pluto may significantly differ from that in Titan's haze.

3. Influx of water and dust

Strobel and Zhu [2] calculated the H₂O mixing ratio of ≈ 10 ppm above 600 km assuming an exogeneous source of H₂O near 500 km and its loss by condensation on the surface and the diffusion-limited thermal escape. The required source was $190 \text{ cm}^{-2} \text{ s}^{-1}$ scaled to the surface, that is, 88 g day^{-1} .

Wong et al. [6] included H₂O and its detailed chemistry in their photochemical model and

calculated the similar H_2O abundances assuming the influx of $2.4 \times 10^6 \text{ cm}^{-2} \text{ s}^{-1}$, that is, 1100 kg day^{-1} . Horanyi et al. [7] estimated ablation of 200 kg day^{-1} of interplanetary dust on Pluto based on the NH and Pioneer 10 and 11 data. However, influxes of water on Saturn, Uranus, and Neptune are $\approx 10^6 \text{ cm}^{-2} \text{ s}^{-1}$ [8] and even greater on Titan ($3 \times 10^6 \text{ cm}^{-2} \text{ s}^{-1}$ [9]) because of the H_2O production from the Saturn rings.

4. Haze

The NH haze observations using LORRI and MVIC were analysed by Gladstone et al. [10]. They proved that the haze particles are fractal aggregates with effective radii of $0.2 \mu\text{m}$ that consist of monomers with radii of $\approx 0.01 \mu\text{m}$. The haze vertical scattering optical depth is 0.013 in the red and the column surface area is 0.02.

The NH solar occultations [1] gave the line-of-sight optical depth of the haze at 180 nm of ≈ 2 near the surface and its vertical optical depth of 0.2 at 180 nm . The difference of a factor of 15 between the UV and red values looks reasonable for very small particles.

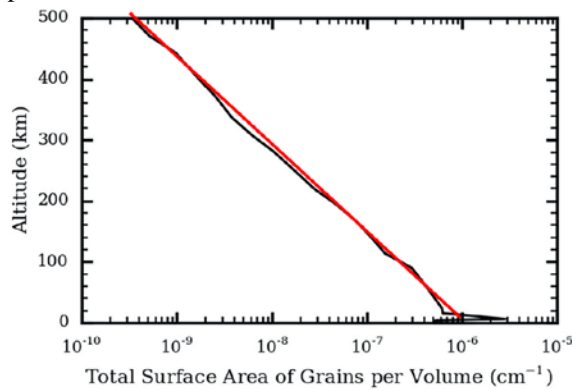


Fig. 2. Volume surface area of the haze in [11]. Red line is the exponential approximation.

However, the haze column surface area in Gao et al. [11] is equal to 8.8 (Fig. 2) and exceeds the value in the red by a factor of 440, though the model [11] is adjusted to fit the haze extinction at 180 nm . The difference may be partly caused by the large mean free path in Pluto's atmosphere, and the spheres of $0.2 \mu\text{m}$ are more appropriate as the condensation centres than the monomers of $0.01 \mu\text{m}$. However, this reduces the difference by a factor of 20 but does not eliminate it.

5. Photochemical models

Two models by Wong et al. [6] and Luspay-Kuti et al. [12] have been developed. Inversions in densities of C_2H_2 , C_2H_4 , and C_2H_6 near 200 km observed in the NH UV solar occultations [1] are identified by Wong et al. as condensation of these species that is effective at $200\text{--}400 \text{ km}$. Sticking coefficients of the condensation process are used as parameters to fit the observations. The highly overestimated haze surface area from Fig. 2 is adopted; however, its effect may be simply corrected by proper scaling of the obtained sticking coefficients.

Luspay-Kuti et al. [12] indicate that the observed C_2H_4 and C_2H_6 cannot condense in Pluto's atmosphere except for a narrow layer near the surface. They substitute condensation by irreversible sticking with coefficients increasing from 0 at the surface to maxima at 400 km . However, the calculated total loss by aerosol trapping is extremely high, $\approx 3 \times 10^{11} \text{ cm}^{-2} \text{ s}^{-1}$ for C_2H_2 in their figure 9, and exceeds the production by three orders of magnitude. This should be incompatible with the observed haze properties. The C_2 hydrocarbon densities near the surface are another set of fitting parameters in the model. The calculated peak total ion density of 30 cm^{-3} is too low compared to $\approx 2500 \text{ cm}^{-3}$ on Titan. Scaling the heliocentric distances, the expected peak density is $\approx 800 \text{ cm}^{-3}$.

Acknowledgement. This work is supported by a grant of Russian Science Foundation to MIPT and V.A. Krasnopolsky.

References

- [1] Young L.A. et al. *Icarus* 300, 174, 2018.
- [2] Strobel D.F., Zhu X., *Icarus* 291, 55, 2017.
- [3] Zhang X. et al. *Nature* 551, 352, 2017.
- [4] Khare B.N. et al. *Icarus* 60, 127, 1984.
- [5] Vinatier S. et al. *Icarus* 219, 5, 2012.
- [6] Wong M.L. et al. *Icarus* 287, 110, 2017.
- [7] Horayi M. et al. *EGU*, Vienna, p. 3652, 2016.
- [8] Feuchtgruber H. et al. *Nature* 389, 159, 1997.
- [9] Krasnopolsky V.A. *Icarus* 236, 189, 2014.
- [10] Gladstone G.R. et al. *Science* 351, aad8866, 2016
- [11] Gao P. et al. *Icarus* 287, 116, 2017.
- [12] Luspay-Kuti A. et al. *MNRAS* 472, 104, 2017.

Ice Giants Exploration: Dual and Twin Spacecraft Approaches

Romolo Politi (1), Diego Turrini (1), Davide Grassi (1), Roberto Peron (1), Valeria Cottini (2), Nicolas Gorius (3)
(1) Institute for Space Astrophysics and Planetology INAF-IAPS, Italy, (2) University of Maryland, College Park, College Park, Maryland, United States (3) NASA Goddard Space Flight Center, Greenbelt, Maryland, United States
(romolo.politi@iaps.inaf.it)

Abstract

With the progression of the robotic exploration of the Solar System and the continuous advance in exoplanetary studies, filling the gap represented by the limited knowledge we possess of Uranus and Neptune is becoming more and more critical. Not only these ice giant planets represent the archetype for studying one of the most abundant classes of exoplanets, but their characteristics and those of their satellite systems have been shaped by the earliest and most violent phases of the life of the Solar System. Understanding them is therefore an essential step in understanding our place in the galactic context. Because of their similarities and differences, both ice giants are compelling targets and much can be learned by their comparative study. With this rationale in mind in 2013 we submitted to the European Space Agency the ODINUS white paper (<http://odinus.iaps.inaf.it>), where we described the scientific case of exploring both planets and their satellites in the framework of a single European L-class mission. To achieve this ambitious goal, we proposed the first mission scenario based on the use of two identical spacecraft to two different planets. Both the scientific case and the original twin orbiter scenario were assessed as feasible by ESA and were further refined and consolidated by the ODINUS team during the following interactions the scientific community. The recent joint NASA-ESA study for future missions to the ice giants (<https://www.lpi.usra.edu/icegiants/>) allowed for confirming the feasibility of the dual/twin spacecraft approach to the two ice giant planets and for considering more ambitious mission profiles, involving larger payloads and the possibility of including atmospheric probes, in the framework of scenarios of international cooperation.

The spectral nature of Titan's major geomorphological surface units: constraints on the composition

A. Solomonidou^{1,2,*}, A. Coustenis³, R.M.C. Lopes², M. Malaska², S. Rodriguez⁴, P. Drossart³, C. Elachi², B. Schmitt⁵, A. Le Gall¹, S. Wall¹, K. Lawrence², N. Altobelli¹, O. Witasse⁹, J. Radebaugh⁶, A. Schoenfeld⁸

¹European Space Agency (ESA), European Space Astronomy Centre (ESAC), Madrid, Spain, ²Jet Propulsion Laboratory, California Institute of Technology, California, USA, ³LESIA - Observatoire de Paris, PSL Research University, CNRS, UPMC Univ. Paris 06, Univ. Paris-Diderot, 92190 Meudon, France, ⁴Laboratoire AIM, Université Paris Diderot, Paris 7/CNRS/CEA-Saclay, DSM/IRFU/Sap, Gif sur Yvette, France, ⁵Institut de Planétologie et d'Astrophysique de Grenoble, Grenoble, France, ⁶Department of Geological Sciences, Brigham Young University, Utah, USA, ⁷Laboratoire Atmosphères, Milieux, Observations Spatiales (LATMOS-UVSQ), Paris, France, ⁸Department of Earth, Planetary, and Space Sciences, University of California, Los Angeles, California, USA, ⁹European Space Agency (ESA), European Space Research and Technology Centre (ESTEC), Noordwijk, Netherlands.

Abstract

We investigate Titan's low-latitude and midlatitude surface using spectro-imaging near-infrared data from Cassini/Visual and Infrared Mapping Spectrometer [1]. We use a radiative transfer code [2-4] to first evaluate atmospheric contributions and then extract the haze and the surface albedo values of major geomorphological units identified in Cassini Synthetic Aperture Radar data, which exhibit quite similar spectral response to the Visual and Infrared Mapping Spectrometer data. We have identified three main categories of albedo values and spectral shapes, indicating significant differences in the composition among the various areas. We compare with linear mixtures of three components (water ice, tholin-like, and a dark material) at different grain sizes. Our fits of the data are overall successful, except in some cases at 0.94, 2.03, and 2.79 μm , indicative of the limitations of our simplistic compositional model and the need for additional components to reproduce Titan's complex surface. Our results show a latitudinal dependence of Titan's surface composition, with water ice being the major constituent at latitudes beyond 30°N and 30°S, while Titan's equatorial region appears to be dominated partly by a tholin-like or by a very dark unknown material. The albedo differences and similarities among the various geomorphological units give insights on the geological processes affecting Titan's surface and, by implication, its interior. We discuss our results in terms of origin and evolution theories.

1. Context/Data

In order to unveil Titan's surface nature, it is important to determine the surface composition of different units, along with their morphological expressions. Matching the surface units with specified mixtures of materials can shed light on the

interconnection between the interior, surface, and atmosphere. The Cassini VIMS obtained spectro-imaging data of Titan's surface from flybys performed during the last thirteen years, in the 0.8-5.2 μm range. The data from the seven narrow methane spectral "windows" centered at 0.93, 1.08, 1.27, 1.59, 2.03, 2.69-2.79 and 5 μm provide some information on the lower atmosphere and the surface parameters. Atmospheric scattering and absorption need to be clearly evaluated before we can extract the surface properties. Here we focus on areas that are in the mid-latitudes and are of geological interest. The geomorphological units and albedo features we analyze are:

- i. the undifferentiated plains [4; 5],
- ii. hummocky/mountainous terrains [4;6],
- iii. labyrinth terrains [6],
- iv. variable plains [5;6],
- v. streak-like plains [6],
- vi. dunes [4;5],
- vii. the Huygens Landing site [6],
- viii. alluvial fans [7], and
- ix. crater ejecta [8].

2. Methods

Our radiative transfer (RT) method is a 1-D multi-stream RT code based on the open-source solver SHDOMPP [2]. As inputs, we used most of the Huygens Atmospheric Structure Instrument (HASI) and the Descent Imager/Spectral Radiometer (DISR) measurements, as well as new methane absorption coefficients. These are important to evaluate the atmospheric contribution and constrain the real surface alterations by comparing the spectra of these regions. Figure 1 shows the spectral variations of the extracted surface albedos from RT of the regions of interest with the 'ground truth' albedo derived at the Huygens landing site (HLS). We then test the surface albedos against a spectral database of Titan candidate ice and organic constituents and provide some

constraints on the possible major material present in every geomorphological unit. We use a new updated material library based on Bernard et al. (2006), Brasse et al. (2015) and the GhoSST database (<http://ghosst.osug.fr>).

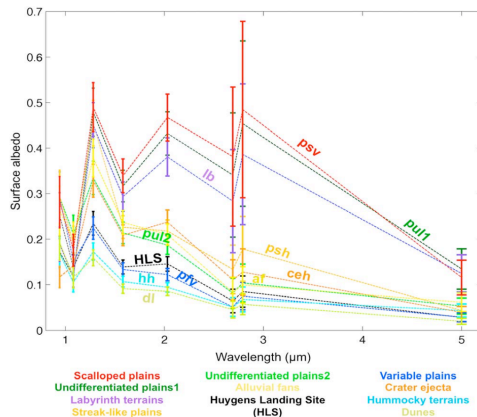


Fig. 1. Weighted averages in the methane windows of the surface albedos of the various geomorphological units: For clarity purposes, we have connected the points with straight lines that do not represent real results but help see the spectral behavior as a whole for each unit.

3. Results

Our results indicate that: i. RoIs with the same geomorphological unit classification also share the same or very similar spectral characteristics, ii. there are three groups of composition mixtures present on Titan's low-latitude and midlatitude surface region. In Figure 2 we plot the regions on an Imaging Science Subsystem global map, and hereafter we compare with previous work and additional insights from geological aspects. Our results suggest the presence of a material compatible with water ice in the areas around high latitudes. The HLS and the variable plains share many albedo characteristics (Figure 1) suggesting that HLS is part of this unit and has an organic origin or is at least coated with organic materials. The same applies to the hummocky terrains and the dunes that are also compatible with an organic surficial composition. The alluvial fans and the crater ejecta units are covered by tholin-like material and seem to be dominated by atmospheric deposits that mask their underlying material. The areas with major constituents spectrally compatible with water ice seem to follow a geographical pattern as all four (northern undifferentiated plains, labyrinths,

scalloped plains, and streak-like plains) are located at northern or southern midlatitudes, close to 30°–60°N and 60°S (Figure 11). Hence, Titan's surface composition has a significant latitudinal dependence.

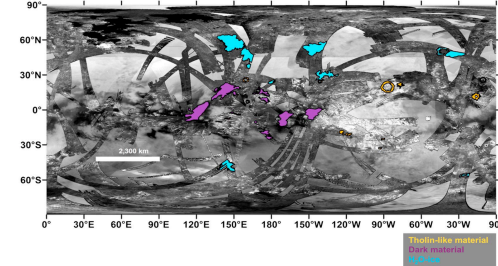


Fig. 2. Implications on the major constituents of Titan regions of interest from Solomonidou et al. 2018 [1].

Taking into consideration our results we provide two possible interpretations: one suggesting that more dark material is being deposited from the atmosphere onto the equatorial regions compared to the higher polar regions and another where we assume that atmospheric deposition is similar in the low-latitude and midlatitude on Titan, but with more rain falling onto the higher latitudes causing additional processing of materials on those regions.

Currently, we are working on deriving information on the full chemical compositions of the aforementioned regions from the extracted surface albedos. This will shed light on the potential formation processes.

Acknowledgements

This research was supported by the Cassini Data Analysis and Participating Scientists Program (CDAPS) grant NH16ZDA001N to R.L. ©2018 California Institute of Technology. Government sponsorship acknowledged.

References

- [1]Solomonidou et al.: JGR, 123, 489-507, 2018. [2]Hirtzig et al.: Icarus, 226, 470-486, 2013. [3]Solomonidou et al.: JGR, 119, 1729-1747, 2014. [4]Solomonidou et al.: Icarus, 270, 85-99, 2016. [4]Lopes et al.: Icarus, 205, 540-558, 2010. [5]Lopes et al.: Icarus, 270, 162-182, 2016. [6]Malaska et al.: Icarus, 270, 130-161, 2016. [7]Radebaugh et al.: Geological Society London, 2016. [8]Neish et al.: GRL, 42, 3746-3754, 2015. [9]Bernard et al.: Icarus, 185, 301-307, 2006. [10]Brasse et al.: PSS, 109, 159-174, 2015.

Evolution of Titan's atmospheric temperature and composition near the poles from Cassini/CIRS

Athena Coustenis¹, Donald E. Jennings², Richard K. Achterberg^{2,3}, Georgios Bampasidis⁴, Conor A. Nixon², Panayotis Lavvas⁵, Valeria Cottini^{2,3}, F. Michael Flasar²

(1) LESIA - Observatoire de Paris, PSL Research University, CNRS, UPMC Univ. Paris 06, Univ. Paris-Diderot, 92190 Meudon, France., (2) Planetary Systems Laboratory, Goddard Space Flight Center, Greenbelt, MD 20771, USA, (3) Department of Astronomy, University of Maryland, College Park, MD 20742, USA, (4) Faculty of Physics, National and Kapodistrian University of Athens, Panepistimioupolis, 15783 Zographos, Athens, Greece., (5) GSMA, Reims Champagne-Ardenne, 51687 Reims, France

Abstract

We will report on the monitoring of seasonal evolution near Titan's poles. Since 2010, we have observed at Titan's south pole a strong temperature decrease and the onset of a dramatic enhancement of several trace species such as complex hydrocarbons and nitriles (HC3N and C6H6 in particular) previously observed only at high northern latitudes (Coustenis et al. 2016 and references therein). This is due to the transition of Titan's seasons from northern winter in 2002 to summer in 2017 and, at the same time, the advent of winter in the south pole. During this transition period species with longer chemical lifetimes linger in the north undergoing slow photochemical destruction, while those with shorter lifetimes decrease and reappear in the south. An opposite effect was expected in the north, but not observed with certainty until now. We present here an analysis of nadir spectra acquired by Cassini/CIRS (Jennings et al., 2017) at high resolution in the past years and describe the temperature and composition variations near Titan's poles. From 2013 until 2016, the northern polar region has shown a temperature increase of 10 K, while the south has shown a more significant decrease (up to 25 K) in a similar period of time. While the south polar region is continuously enhanced since about 2012, the chemical content in the north is finally showing a clear depletion for most molecules only since 2015 (Coustenis et al., 2017, submitted for publication). This can set constraints on photochemical and GCM models.

1. Observations and analysis

For the purpose of this article, we exploited CIRS high spectral resolution (0.5 cm⁻¹) data taken from 2012 to 2016 in the surface-intercepting nadir mode. CIRS is a Fourier transform spectrometer spanning 10 to 1500 cm⁻¹ in three spectral channels or Focal Planes (FP). We use here spectra from the far-

infrared FP3 and FP4 that cover the 600-1500 cm⁻¹ range (Jennings et al. 2017).

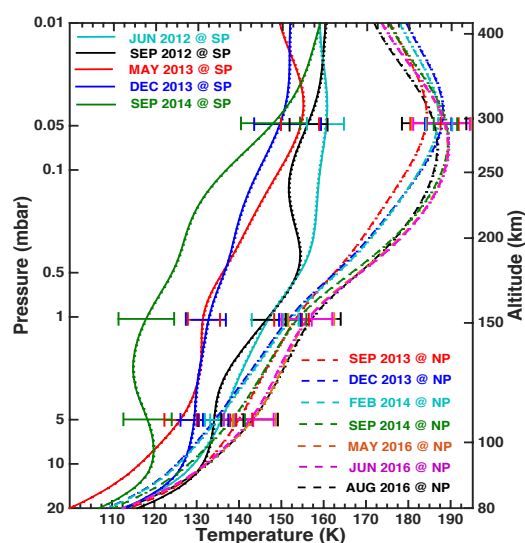


Fig. 1. Temperature evolution in Titan's stratosphere near the poles from 2012 to 2016. The southern polar profiles are shown in full lines, while the north pole profiles are depicted in dashed lines and the different dates are indicated in different colors. 3- σ uncertainties are shown.

For the purpose of this article, we exploited CIRS high spectral resolution (0.5 cm⁻¹) data taken from 2012 to 2016 in the surface-intercepting nadir mode. CIRS is a Fourier transform spectrometer spanning 10 to 1500 cm⁻¹ in three spectral channels or Focal Planes (FP). We use here spectra from the far-infrared FP3 and FP4 that cover the 600-1500 cm⁻¹ range (Jennings et al. 2017).

2. Results

In our recent publications (Coustenis et al. 2016; 2018), we inferred the temperature profiles and the chemical composition at different dates from 2010 and up to 2014 for high northern and southern latitudes (at and beyond 50°N and 50°S).

We derive the temperature profile from the methane n4 band and then apply the ARTT code to the rest of the spectrum to extract the abundances of the weak gases.

We had already shown in Coustenis et al. (2016) that as the southern hemisphere moved into winter after 2010, large temperature variations were observed near the south pole (70°S) in the stratosphere (from 0.1 down to 1 mbar pressure levels). Indeed, while a moderate warming is observed in the summer-entering north for the mid and high northern latitudes, a decrease of about 10-15 K in temperature was measured already for the 50°S latitudes. A more spectacular drop in temperature by as much as 25 K at 70°S was measured from 2012 to 2014. These temperature variations were accompanied by a strong enhancement of chemical compounds in the south polar region, while the north failed to show the opposite effect, which indicated a non-symmetrical reaction to the seasonal influence for each pole. We explore here more recent dates seeking to determine longer-term seasonal effects near Titan's poles.

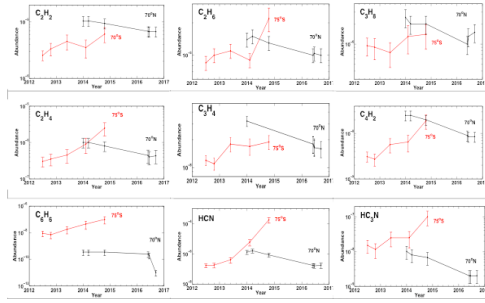


Fig. 2. Retrieved abundances of trace gases above Titan's poles.

More recent data now focusing at the poles : our radiative transfer results at high Northern latitudes (at about 20° from the pole), show that the North pole is now becoming significantly depleted in trace gases. This occurs essentially after 2015. Not much difference again is found for CO₂ (not shown in this

figure). Limited drop in mixing ratios within error bars is measured for the other most abundant molecules resisting the photolysis (like C₃H₈, C₂H₆, C₂H₂ or C₂H₄). However, the trend for a drop in content for these molecules is attested by the consistent lower values found for these species in all 2016 spectral averages wrt 2014.

References

- [1] Coustenis et al., 2016, Icarus 270, 409-420
- [2] Jennings et al., 2017, Applied Optics 56, no 18, 5274-5294.
- [3] Coustenis et al. 2018. Astroph. J., Lett., 854, no2

Stellar Occultation of Triton on October 5th, 2017

Joana Oliveira (1), Bruno Sicardy (1), Erick Meza (1), Josselin Desmars (1), Jean Lecacheux (1), Marcelo Assafin (2,3), Julio Camargo (2), Jose-Luis Ortiz (4), Pablo Santos-Sanz (4), Wolfgang Beisker (5), Mike Kretlow (5), Rodrigo Leiva (6), Diane Bérard (1), the Rio and Granada occultation teams, the IOTA teams (Europe and USA), the Triton occultation teams (1) LESIA/Observatoire de Paris, CNRS UMR 8109, Sorbonne Université, Université Paris-Diderot, 5 place Jules Janssen, F-92195 Meudon Cédex, France, (2) ON Rio de Janeiro, (3) OV/UFRJ Rio de Janeiro, (4) IAA Granada, (5) IOTA Europe, (6) SWRI Boulder (joana.oliveira@obspm.fr)

Abstract

On October 5th, 2017, a stellar occultation by Triton was observed from over 80 sites in Europe, North Africa, and USA, by both professional and amateur astronomers. These observations provide unique information on the thermal structure of Triton's atmosphere and its evolution since the Voyager 2 observations in 1989. A noteworthy feature observed in about 25 light curves is the so-called central flash, corresponding to an increase of brightness in the middle of the event. We will present preliminary results derived from this event, in particular a comparison of the pressure obtained at prescribed levels, with results from previous observations. Constraints on the atmosphere shape derived from the central flashes will be given.

1. Introduction

Triton is the largest of Neptune's satellites with a radius of 1353 km. It is the only satellite, other than Titan, to possess a significant atmosphere. Its atmosphere (mainly composed of molecular nitrogen N_2) is special as it is in vapor pressure equilibrium with the N_2 frost at the surface. The NASA/Voyager radio experiment provided a surface pressure of $p_{\text{surf}} \sim 16 \mu\text{bar}$ in 1989 [1], consistent with vapor equilibrium with a surface at $T_{\text{surf}} \sim 40 \text{ K}$. The sensitivity of p_{surf} to T_{surf} is very high, as each increment $\Delta T = 1 \text{ K}$ corresponds to an increase by a factor of two in pressure. In that context, seasonal effects are of paramount importance: in fact, due to the large variations of the sub-solar latitude, very different terrains are illuminated as time changes (Fig. 1). The decades 1990-2000 were exceptional due to an "extreme solstice", where southern latitudes of up to 50° S were directly illuminated by the Sun. This happens every 650 years, due to a combination of Neptune's heliocentric motion and Triton orbital precession. Since 1989, the Voyager

data, combined with a few ground-based stellar occultations suggest that Triton's atmospheric pressure increased by a factor of about two. This increase could stem from the sublimation of N_2 ice deposited on Triton's southern polar cap [2].

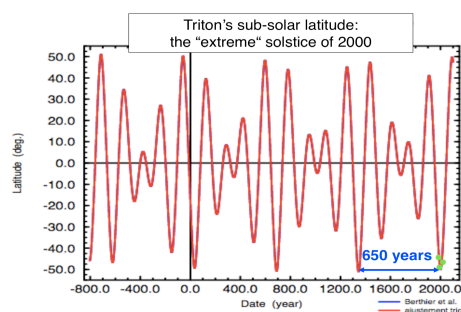


Figure 1 - Triton's subsolar latitude vs. time. Note the exceptional character of the 2000 solstice.

2. The event

This stellar occultation was unique, as it was the first one favourable since 1997. Thanks to a pre-release of the Gaia DR2 star positions around Triton, the final prediction was about 3 milli-arcsecond from the actual shadow path. It involved a bright star ($V = 12$) and densely populated areas in terms of observing sites, including amateurs. It was visible from a large part of Europe and Northern Africa, as well as from eastern USA (Fig. 2), resulting in a dense coverage of Triton's atmosphere (Fig. 3).

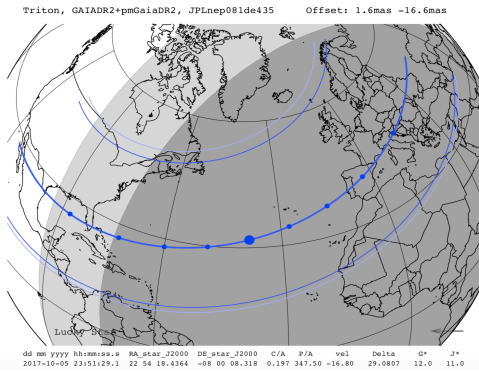


Figure 2 - Path of Triton's shadow during the event.

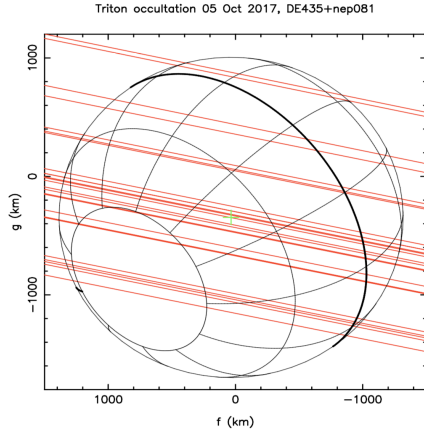


Figure 3 – Occultation chords for 26 stations across Triton's atmosphere. The green cross marks Triton's center.

3. Preliminary results

Refraction of stellar rays by the atmosphere causes a stellar flux drop (Fig. 4), which provides Triton's atmospheric profiles (density, temperature, pressure, including p_{surf}) from altitudes of 10 km (7 μbar) to about 100 km (0.1 μbar). Stations near centrality experienced the so-called central flash (Fig. 4) which constraints the sphericity of Triton's atmosphere and possible presence of hazes. Moreover, combining all observations, one can perform a fit to all the light curves and derive global properties of the atmosphere.

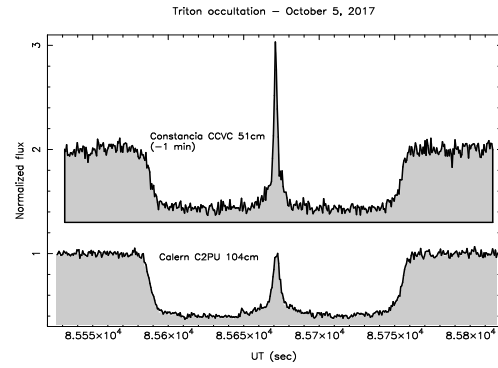


Figure 4 - The occultation event and central flash observed at two stations: south-east France and Constância in Portugal. The total duration of the event is about 3 minutes.

In particular, we will discuss the evolution of Triton's atmospheric pressure from 1989 up to present, as well as the upper limit for the atmospheric oblateness using the central flash, from which constraints on zonal winds and hazes will be given.

Acknowledgements

This work has received support from the Portuguese Foundation for Science and Technology (FCT) through the PhD grant SFRH/BD/131700/2017. The work leading to these results has also received funding from the European Research Council under the European Community's H2020 2014-2020 ERC grant Agreement n° 669416 "Lucky Star". We acknowledge the Gaia project for pre-releasing DR2 stellar positions that greatly improved the prediction of the event.

References

- [1] Tyler et al.: "Voyager radio science observations of Neptune and Triton", *Science* 246, 1466, 1989.
- [2] Elliot et al.: "Global warming on Triton", *Nature* 393, 765, 1998.

A new polar storm and a long-lived equatorial disturbance in Saturn's post-Cassini era

A. Sánchez-Lavega (1), R. Hueso (1), J. F. Rojas (1), T. del Río-Gaztelurrutia (1), E. García-Melendo (2), M. Soria Guerrero (2), J. Legarreta (1), A. A. Simon (3), M. Wong (4), J. M. Gómez-Forrellad (5), M. Delcroix (6) and the Observers Team (7)

(1) Escuela de Ingeniería de Bilbao, UPV/EHU, Bilbao, Spain, (2) Escola Superior d'Enginyeries Industrial, Aeroespacial i Audiovisual, UPC, Terrasa, Spain, (3) NASA Goddard Space Flight Center, Greenbelt, MD, USA, (4) University of California Berkeley, Berkeley, CA, USA, (5) Fundació Observatori Esteve Duran, Barcelona, Spain, (6) Société Astronomique de France, Paris, France, (7) Observers Team (contributing to PVOL database): M. Bassani Sparrenberger, T. Barry, D. Peach, E. Morales, P. Miles, A. Wesley, D. P. Milika & Nicholas, M. Kardasis, C. Foster, C. Go, T. Olivetti, A. Casely, W. Martins (agustin.sanchez@ehu.eus).

Abstract

We report on a new bright spot discovered by amateur astronomers on Saturn's atmosphere on March 29, 2018 at planetographic latitude $+66.8^\circ\text{N}$. The spot moved with a mean velocity of $+60.9\text{ ms}^{-1}$ and showed brightening episodes during the observing period. Eastward and westward of it smaller spots were seen allowing the measurement of the wind speeds in the area that differs from the mean wind velocity profile determined at this latitude [1] [2]. We also report on the continuing observation of the bright spot at latitude $+6^\circ\text{N}$ [3] that holds the longevity record for a feature in Saturn's Equator (> 4 years). Its mean velocity of 449 ms^{-1} has remained stable during this period within $\pm 3\text{ ms}^{-1}$.

1. Introduction

Besides the Great White Spots (GWS), huge planetary-scale storms that represent rare and exceptional cases, with only 6 events reported from 1876 to date [4], the presence in Saturn's atmosphere of high albedo spots that are observable with small telescopes is an unusual phenomenon. The study of these bright spots allows characterizing both the properties of the most significant storms and the cycles of activity at different latitudes in the planet. Here we report a study of two bright spots observed at two different latitudes of Saturn after the end of the Cassini mission in mid-September 2017. One is a new spot observed in the northern polar area, in the region of a singular double-jet (50°N to 70°N) that has no a symmetric counterpart in the south [1]. The second is a long-lived equatorial storm that shows a remarkable stability in size and velocity [3].

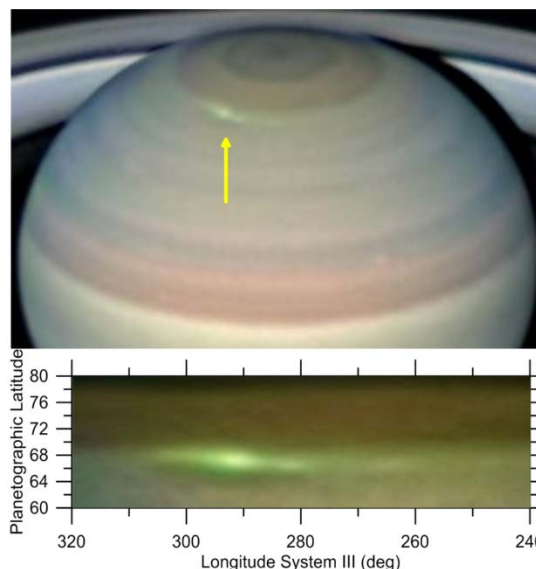


Figure 1: The polar spot in expansion as observed by Damian Peach on April 1, 2018.

2. The polar storm

On March 29th, 2018, a high albedo spot (WS) was observed in the northern polar area (Figure 1, 3). It emerged in the latitude of a double jet where a system of three coupled vortices (ACA) had been reported previously, and where a disturbance took place in 2015 [5]. We tracked WS from 29 March to 2 May on 57 selected images obtained by 20 observers and submitted to PVOL [6] and ALPO Japan [7] image repositories. WS mean longitude drift was $-11.6^\circ/\text{day}$ in System III and its mean planetographic latitude $+66.8^\circ \pm 0.5^\circ\text{N}$ resulting in a mean zonal velocity of $+60.9\text{ ms}^{-1}$. The tracking of this longitudinal drift back

in time shows that a good correlation exists with the position of a cyclone seen in the Cassini epoch north of the ACA system, suggesting that WS could have originated inside that cyclone. In our measurements, WS had an extent of $\sim 10^\circ$ (zonal) and 4° (meridional), acquiring in the first days an S-shape with a pattern of nearby spots (Fig. 1) suggestive of the development of a disturbance. The velocity of these features reveals differences with the wind profile at this latitude (Fig. 2) [1, 2]. Numerical simulations of the storm dynamics are being developed.

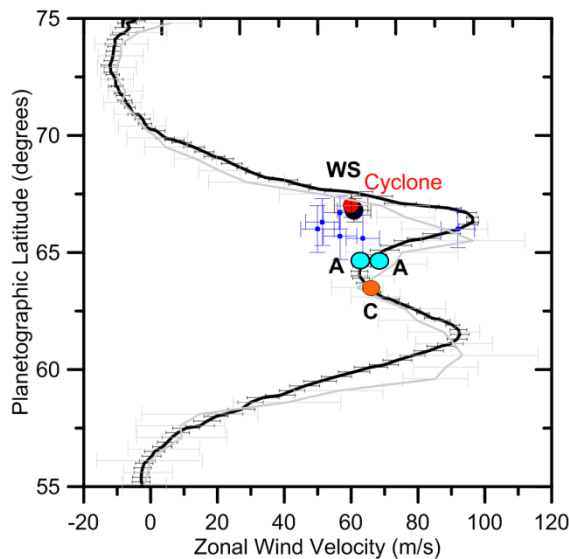


Figure 2: Velocities in the double jet. Continuous profiles: black from Cassini ISS [1], gray from Voyager 1-2 [2]. The WS (bright polar spot) is the back dot and the blue dots are from related features in 2018. The cyclone and ACA velocities are from Cassini ISS [4].

3. The long-lived Equatorial Storm

The storm at latitude $+6^\circ\text{N}$ reported in [3] has been observed recurrently during the Saturn oppositions in 2016, 2017 and 2018 (Figure 3), thus becoming the feature with the longest lifetime ever observed in Saturn's Equator. Tracking of the feature during this period resulted in a wind speed ranging from 446.3 ms^{-1} to 451.8 ms^{-1} . In images with high enough resolution, the feature is seen to be double, with a northern and southern components moving coherently. No explanation exists yet for the nature of this unusual feature.

New observations of Saturn are planned for June 6, 2018 within the OPAL program of Hubble Space Telescope. Those new images will provide additional information on both phenomena.



Figure 3: The arrow shows the polar spot (WS) and the ellipse encloses the long-lived storm in the Equatorial Zone as imaged by A. Wesley on April 5, 2018.

Acknowledgements

This work has been supported by the Spanish MINECO project AYA2015-65041-P, MINECO/FEDER (UE), and Grupos Gobierno Vasco IT-765-13.

References

- [1] E. García-Melendo et al: Saturn's zonal wind profile in 2004 - 2009 from Cassini ISS images and its long-term variability, *Icarus*, 215, 62-74 (2011)
- [2] A. Sánchez-Lavega et al: Saturn's zonal winds at cloud level, *Icarus*, 147, 405-420 (2000)
- [3] A. Sánchez-Lavega et al: An Enduring rapidly moving storm as a guide to Saturn's equatorial jet complex structure, *Nature Communications*, 7:13262 (2016)
- [4] A. Sánchez-Lavega et al: Deep winds beneath Saturn's upper clouds from a seasonal long-lived planetary-scale storm, *Nature*, 475, 71-74 (2011)
- [5] T. del Río-Gaztelurrutia et al: A planetary-scale disturbance in a long living three vortex coupled system in Saturn's atmosphere, *Icarus*, 302, 499-513 (2018)
- [6] PVOL: <http://pvol2.ehu.eus/pvol2/>
- [7] ALPO Japan: <http://alpo-j.asahikawa-med.ac.jp/Latest/Saturn.htm>

UV irradiation of Titan organic haze

Nathalie Carrasco (1), Sarah Tigrine (1, 2), Lisseth Gavilan (1), Laurent Nahon (2) and Murthy Gudipati (3)
(1) LATMOS/IPSL, UVSQ, Université Paris-Saclay, UPMC Univ. Paris 06, CNRS, France, (2) SOLEIL synchrotron, France, (3) Jet Propulsion Laboratory, Science Division, California Institute of Technology, USA (nathalie.carrasco@uvsq.fr)

Abstract

The Cassini-Huygens space mission discovered that Titan's thick brownish haze is initiated high in the atmosphere at an altitude of about 1000 km. So far, nothing is known on the possible photochemical evolution of the organic aerosols composing the haze. Here, we address this aging process, simulating in the laboratory how solar vacuum ultraviolet irradiation affects the aerosols. The chemical evolution is monitored by infrared spectroscopy.

1. Introduction

After their production in the ionosphere [1], Titan's aerosols are known to evolve through microphysics during their sedimentation down to Titan's surface [2]. As laboratory analogs of Titan's atmospheric aerosols (tholins) are strong UV absorbers [3], UV irradiation is suspected to induce a chemical evolution of Titan's aerosols during their descent in the atmosphere. The aim of this work is to simulate this irradiation process on Titan's aerosols and to address the impact on the chemical composition of the organic solids [4]. We have chosen two irradiation wavelengths to experimentally simulate the evolution of the aerosols high in the atmosphere: 95 nm representative of hard photons at about 1000 km and 121.6 nm (Lyman- α) a major VUV contribution in the solar spectrum penetrating down to 600 km.

2. Methodology

2.1 Sample synthesis

First tholins were produced in a 95-5% N_2 - CH_4 radio-frequency plasma discharge as thin organic films of 440 ± 20 nm thicknesses deposited onto Silicon windows (with a surface of 11 mm² and a thickness of 0.5 mm). Film thickness was found by

spectroscopic ellipsometry in the 370–1000 nm spectral range (M-2000V, Woollam Co).

1.2 VUV irradiation source

The 11-mm²-sample surface is entirely illuminated by the beam spot of the quasi-monochromatic DESIRS-synchrotron beamline [5]. Each sample is irradiated with a specific wavelength (95 or 121.6 nm) and a chosen irradiation-duration. With the chosen experimental configuration, the photon flux density is two orders of magnitude larger than the corresponding UV solar flux density. The dose is adjusted by choosing shorter irradiation times of typically a few hours in our experiments, in order to simulate approximately one-Titan day irradiation.

1.3 IR spectroscopy

The samples were characterized by ex-situ mid-IR absorption spectroscopy in the 1200–3500 cm⁻¹ wavenumber range. All pre- and post-irradiation infrared measurements were performed by transmission analysis with the Thermo Scientific Nicolet iN10 MX spectrometer at the SMIS beamline of the synchrotron SOLEIL facility with a mercury cadmium telluride and a spectral resolution of 4 cm⁻¹.

3. Results

The effect of VUV irradiation is illustrated in Figure 1 with the comparison of the absorbance spectra of a single sample before and after 24 hours irradiation at 121.6 nm. We observe a decrease of the nitrile functions, C-H bonds and N-H bonds. The samples irradiated at 95 nm evolve similarly, with significant changes only observed at shorter irradiation durations for the nitrile functional group. As expected with the higher energy dose provided at 95 nm, absorption of the nitrile group decreases faster and more significant with 95 nm irradiation than with 121.6 nm. A loss of

about 20% is obtained at 95 nm after 2 hours of irradiation, which is about twice compared to the one observed at 121.6 nm.

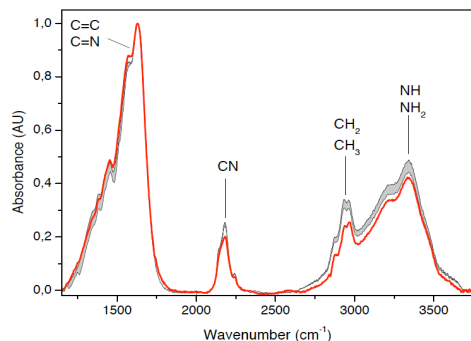


Figure 1: Infrared absorption spectra normalized to the highest absorption value at $\sim 1550\text{ cm}^{-1}$. The grey envelope shows the dispersion (2σ) of the non-irradiated sample in the $1200\text{--}3500\text{ cm}^{-1}$ range. The red spectrum is recorded after irradiation for 24h by VUV photons at 121.6 nm [4].

The penetration depth of the VUV radiation is about 20 nm in our organic sample (obtained from the imaginary part k of the VUV refractive index [6]). The effective layer thickness affected by the radiation is considered at four times the penetration depth with a residual radiation of 2%. The short penetration depth of VUV photons means that these photons are effective up to 100 nm of the 440 nm thick sample during VUV irradiation. The experimental 15-20% IR signature attenuation observed on Figure 1 is similar to the thickness contribution of the irradiated layer, showing that the irradiated layer possesses totally different IR properties from the non-irradiated layer.

4. Summary and Conclusions

This work provides evidence that VUV photochemistry with wavelengths below 150 nm could in particular deplete the sensible primary and secondary amine functions of aerosols in the upper atmosphere. This would be consistent with the VIMS measurements in the stratosphere [7], which show no evidence of these functions. The irradiation effect does preserve nitrogen-bearing functionalities that are more strongly bound in the aerosol skeleton, such as tertiary amines, imines and nitriles (except

conjugated nitriles). This chemical transformation of the aerosol composition would thus allow the VIMS results to agree with the high nitrogen content reported by the Huygens-ACP instrument close to the surface [8].

Acknowledgements

N.C. and L.G. thank the European Research Council for funding via the ERC PrimChem project (grant agreement 636829). S.T. acknowledges the University of Paris-Saclay for thesis funding. The work of M.S.G. at the Jet Propulsion Laboratory, California Institute of Technology was performed under the NASA-SSW grant 'Photochemical Processes in Titan's Atmosphere'. L.N. acknowledges support from the Agence Nationale de la Recherche (ANR-07-BLAN-0293).

References

- [1] Waite et al., *Science*, Vol. 316, p. 870-875, 2007.
- [2] Lavvas et al., *Astrophysical Journal*, Vol. 728, p.80, 2011.
- [3] Mahjoub et al., *Icarus*, Vol. 221, p. 670, 2012.
- [4] Carrasco et al. *Nature Astronomy*, available online, 10.1038/s41550-018-0439-7, 2018.
- [5] Nahon et al., *J. Synchrotron Rad.* Vol. 19, pp. 508-520, 2012.
- [6] Khare, B. N. et al. *Icarus*, Vol. 60, pp.127-137, 1984.
- [7] Kim, S. J. et al. *Planetary and Space Science*, Vol. 59, 699-704, 2011.
- [8] Israel, G. et al. *Nature*, Vol. 438, pp. 796-799, 2005.

Experimental study of ammonia formation in Titan's ionosphere

A. Chatain (1,2), N. Carrasco (1), O. Guaitella (2), M. Napoleoni (1), L. Vettier (1), G. Cernogora (1)
(1) LATMOS, CNRS, Université Versailles St-Quentin, Sorbonne Universités, 78280 Guyancourt, France
(2) LPP, CNRS, Ecole Polytechnique, Sorbonne Universités, Université Paris XI, 91128 Palaiseau, France
(audrey.chatain@latmos.ipsl.fr)

Abstract

Ammonia is an interesting molecule suspected to be formed in Titan ionosphere and leading to further complex chemistry. Here we experimentally study one of the two ways of formation of ammonia in the ionosphere: the catalysis on surfaces in a N_2 - H_2 plasma. We vary plasma conditions in a CCP RF discharge and follow the ammonia formation thanks to IR and mass spectrometries. We show the strong effect of pressure, H_2 percentage, plasma power and metallic surfaces.

1. Introduction

Titan's ionosphere is the place of complex gas chemistry. The interaction of the major species N_2 , CH_4 and H_2 with the surrounding plasma leads to the formation of new molecules. Here we study the formation of ammonia, which has a great role for further chemical reactions [1]. However, data of the Cassini-Huygens mission are complex to interpret concerning ammonia. Neutral mass spectrometry at low masses is blurred by molecule splitting and the explanation of the detection of the ion NH_4^+ is still under debate [2].

In such cases laboratory simulation can be useful to get clues on the chemistry going on. Ammonia has been detected in experiments simulating Titan's ionosphere [3]. Two different chemical paths have been spotted to form ammonia: with carbon chemistry in the gas phase or without carbon but using surfaces, which can be nanograins or walls. As a first step here we simplify the system to study only the influence of surfaces. A radiofrequency Capacitively Coupled Plasma (CCP RF) discharge is ignited in a N_2 - H_2 mixture simulating Titan's ionosphere without carbon. The evolution of the system is diagnosed with infrared absorption spectroscopy, neutral and positive ion mass spectrometry. We looked at the influence of pressure, H_2 percentage and power.

2. Experimental device

2.1 Plasma reactor - PAMPRE

A cylindrical stainless steel chamber is used to reproduce Titan atmospheric conditions [3]. It is 40cm high and 30cm in diameter. A N_2 - H_2 gas mixture with 0 to 5% of H_2 is injected in the chamber at up to 55sccm, varying the pressure up to 1mbar.

The CCP RF discharge is confined in a smaller cylindrical box of 13.6cm in diameter, inside the chamber. We studied cases with electrodes RF potential tuned up to 460V in peak to peak amplitude.

2.2 IR spectrometry

Ammonia formed in the chamber is quantified by IR absorption spectroscopy with a Nicolet 6700 Fischer FTIR spectrometer. The measurement is directly done during the discharge, and the absorption length is the diameter of the chamber. An accumulation of 5000 scans is needed to obtain a reasonably high signal to noise ratio at $2cm^{-1}$ resolution, which takes 2 to 3 hours.

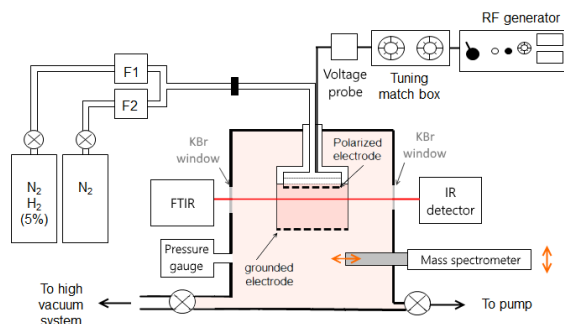


Figure 1: plasma reactor and diagnoses

2.3 Mass spectrometry

In order to better characterize the evolution of ammonia concentration along time and space, we use a mass spectrometer of Hiden EQP series. It is calibrated thanks to IR measurements.

The spectrometer is also used to detect positive ions. For this measurement, the collector head is put in contact with the internal box, in which we drilled a hole to let ions out to the spectrometer without disturbing the ground configuration.

3. Results

3.1 Influence of H₂ percentage

All measurements agree on the strong role of H₂ amount on the formation of ammonia and its ions.

First IR results show a linear dependence of ammonia formation with the H₂ amount in the gas phase. It reaches about $3 \cdot 10^{13} \text{ cm}^{-3}$ for 5% of H₂ in N₂ at 0.92mbar.

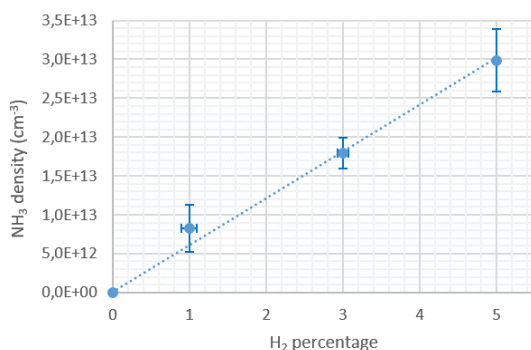


Figure 2: Quantification of ammonia with IR absorption spectrometry at 0.92mbar and 30W.

3.2 Sensitivity to plasma parameters

With the mass spectrometer, we show that ammonia formation is strongly sensitive to plasma parameters. The ammonia to nitrogen ratio increases by about 40% when we increase the peak-to-peak RF voltage of 100V for 0.92mbar of N₂-H₂ at 5%. It doubles when the pressure drops from 0.92mbar to 0.36mbar. When the central box is removed, the quantity of ammonia is divided by two.

3.3 Positive ions

Positive ion populations change quickly as soon as some hydrogen is added into the reactor. N₂⁺, N⁺, N₃⁺ and N₄⁺ here in pure N₂ decrease and are replaced by N₂H⁺, NH₄⁺, NH₃⁺, H₃⁺...

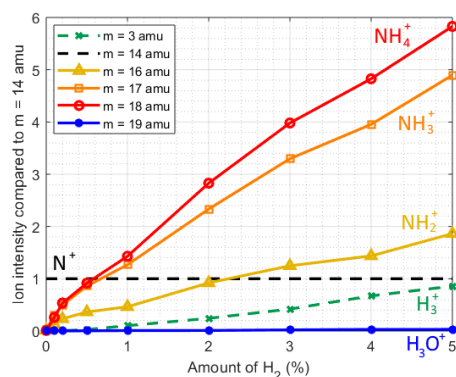


Figure 3: Relative ion intensities as function of H₂ percentage at 0.91mbar and 30W

4. Perspectives

Here we studied the formation of ammonia on the planar metallic surfaces of the reactor. The next step to understand ammonia formation on Titan will be to add methane in the gas mixture to quantify the chemical path using carbon to form ammonia. The formation of aerosols inside the chamber will also complex the study, giving new surfaces to create ammonia according to the first chemical path.

Acknowledgements

NC acknowledges the financial support of the European Research Council (ERC Starting Grant PRIMCHEM, Grant agreement no. 636829).

AC is grateful to the doctoral program of ENS Paris-Saclay for its financial support.

References

- [1] Yelle, R. V., Vuitton, V., Lavvas, P. et al. Formation of NH₃ and CH₂NH in Titan's upper atmosphere. *Faraday discussions*, 147, 31-49, 2010
- [2] Dobrijevic, M., Loison, J. C. et al. 1D-coupled photochemical model of neutrals, cations and anions in the atmosphere of Titan. *Icarus*, 268, 313-339, 2016
- [3] Carrasco, N., Gautier, T. et al. Volatile products controlling Titan's tholins production. *Icarus*, 219(1), 230-240, 2012

The deep winds of Jupiter and Saturn as inferred from recent gravity measurements - similarities and differences

Eli Galanti (1), Yohai Kaspi (1), Daniele Durante (2), Paolo Racioppa (2), and Luciano Iess (2)
(1) Weizmann Institute of Science, Rehovot, Israel, (2) Sapienza Università di Roma, Rome, Italy.

Abstract

The two gas giants of the Solar System, Jupiter and Saturn, exhibit strong zonal flows at the cloud level. The Jupiter winds consist of strong zonal jets (up to 140m/s) alternating latitudinally between eastward and westward jets, and have a significant asymmetric component between the northern and southern hemispheres. On Saturn, the wind pattern is a wide and mostly symmetric eastward flow of nearly 500 m/s at the equatorial region, and smaller scale jets extend to high latitudes. But how deep these winds penetrate into the planets interior remained a fundamental open question until recently, when both Juno at Jupiter and Cassini at Saturn enabled answering this decades long question.

The gravity experiments, performed by both spacecrafts, provided measurements of the gravity harmonics with unprecedented accuracy. They brought into light substantial differences between the two planets. The Jupiter's even gravity harmonics were found to follow closely those predicted by rigid body models and its odd harmonics to be large, clearly above the measurement uncertainty level. Conversely, the even harmonics in Saturn deviate considerably from those predicted by rigid body models, especially for harmonics larger than J4, and its odd harmonics turned out small with only J5 being substantially above the uncertainty level. Another remarkable difference is a small but clearly detectable part of Saturn's gravity that has no counterpart on Jupiter and whose nature is currently unknown.

Using the gravity measurements, together with an adjoint based inverse model of the flow dynamics, we find that on both planets the winds are very deep - reaching around 3,000km on Jupiter and even deeper on Saturn. This points to some similarities and differences on both planets. In both planets the winds observed at the cloud level are a manifestation of deep flows extending thousands of kilometers deep. With that, the differences are striking. The winds on Saturn, a planet smaller than Jupiter, penetrate 3 times deeper and are much more symmetric than the winds on Jupiter. The winds on Jupiter, penetrating to lesser depths, seems to be less connected between the hemispheres, and thus allowing stronger asymmetries to evolve. These differences are likely the result of Saturn having a 3 times smaller and a much weaker magnetic field.

In the presentation we will discuss the gravity measurements, the depth of the winds analysis, and the implications to the characteristics of the two planets.

Pluto's and Triton's hazes

Panayotis Lavvas

GSMA/Université de Reims Champagne Ardenne, CNRS (panayotis.lavvas@univ-reims.fr)

Abstract

Observations from *New Horizons* instruments revealed the presence of photochemical hazes in Pluto's atmosphere [1], while *Voyager 2* observations have demonstrated that similar hazes are also present in the similar atmosphere of Triton [2,3]. Detailed modelling of the atmospheric photo-chemistry of these atmospheres allow to evaluate the mechanism behind the formation of these hazes, while simulations of the involved microphysics permit a calculation of the particle properties that can be validated against the available observations. The results of these studies demonstrate the similarities and the differences for the hazes of these atmospheres, while comparison to the photochemical hazes of Titan's atmosphere [4] provide a global picture of aerosol formation at different conditions.

References

- [1] Gladstone et al. 2016. The atmosphere of Pluto as observed by New Horizons, *Science*, 351, aad8866
- [2] Pollack, JB et al. 1990. Scatterers in Triton's atmosphere: Implications for the seasonal volatile cycle. *Science*, 250,440-443
- [3] Rages, K and Pollack, JB, 1992. Voyager imaging of Triton's clouds and hazes. *Icarus*, 99, 289-301.
- [4] Lavvas P., et al. (2013). Aerosol growth in Titan's ionosphere. *PNAS*, 110(8), 2729-2734.

Formation of Saturn's small inner moons by collisions of similar-sized moonlets

Adrien Leleu (1,2), Martin Jutzi (1) and Martin Rubin (1)

(1) Physics Institute, Space Research and Planetary Sciences, Center for Space and Habitability - NCCR PlanetS - University of Bern, Switzerland

(2) IMCCE, Observatoire de Paris - PSL Research University, UPMC Univ. Paris 06, Univ. Lille 1, CNRS, 77 Avenue Denfert-Rochereau, 75014 Paris, France

(adrien.leleu@space.unibe.ch)

Abstract

The Cassini spacecraft revealed the spectacular, highly irregular shapes of the small inner moons of Saturn, ranging from the unique “ravioli-like” forms of Pan and Atlas to the highly elongated structure of Prometheus. Closest to Saturn, these bodies provide important clues regarding the formation process of small moons in close orbits around their host planet. By the means of N-body and Smooth Particle Hydrodynamics (SPH) simulations, we show that the range of shapes of these small moons is a natural byproduct of mergers of similar-sized moonlets, with impact parameters and velocities that are consistent the current orbits of the small moons.

1. Introduction

The small inner moons Atlas, Prometheus, Pandora, Janus, and Epimetheus are repelled by the rings of Saturn at a rate that is proportional to their mass and decreases with their distance [1,2]. It has thus been proposed that these moons were formed in a pyramidal regime (i.e. by a series of mergers of similar sized bodies) as they migrated away from the rings [2,3]. This scenario is supported by the observations of the small inner Saturnian satellites, as bodies with similar semi-major axis have comparable masses: $m_{\text{Prometheus}}/m_{\text{Pandora}} \sim 1.16$ and $m_{\text{Janus}}/m_{\text{Epimetheus}} \sim 3.6$ (JPL SSD, not accounting for error bars), and the mass of these bodies increase with their distance to the rings. The pyramidal regime provides an alternative to the formation by gradual accretion of small aggregates of ring material onto a proto-moon. The later scenario would result in Roche ellipsoids [4,5], not consistent with the observed shapes of the small moons (see Figure 1). For instance, while Atlas and Pan require a mechanism that makes their shapes

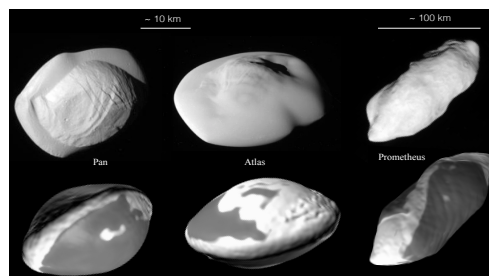


Figure 1: Top: Cassini observations (CREDIT: NASA/KPL-Caltech/Space Science Institute). Bottom: outcome of the simulations.

Flatter [5], Prometheus is over-elongated and its long axis extends beyond the Roche lobe [4].

2. Method

We developed a model for the late stages of the formation of the small inner moons of Saturn from Pan to Janus and Epimetheus, assuming that they formed in the pyramidal regime [2,3]. We investigate if the shapes resulting from the final collisional mergers are consistent with the current shapes of these moons. To this end, we combine N-body simulations to estimate the possible range of impact angles and velocities between the precursors of a given moon, and Smooth Particle Hydrodynamics (SPH) simulations to obtain the outcome of the collisions.

First, a general study of the evolution of the orbit of two moonlets was conducted, using 3-body integrations, taking into account the oblateness of Saturn, the effect of the rings and the presence of larger moons. From it, we derived likely impact

velocities and impact parameters for the collision. We then used SPH simulation to study these collisions, taking into account the Coriolis forces and tides raised by Saturn. Depending on the parameters of the impact, we identified two regimes: mergers, resulting in a variety of shapes, and hit-and-runs, where two distinct bodies resulted from the encounter.

Finally, we ran several populations of N-body simulations, using the prescriptions derived from the SPH simulations whenever a collision occurred. Integration stopped when a merger occurred, or when subsequent hit-and-run reduced the mass of the moonlet below a given threshold.

3. Results

The range of impact velocities and impact angles that are derived from the orbital evolution of the precursor of the moonlet leads to a range of shapes (Figure 1). Close to head-on impacts lead to flattened structures with large-scale ridges, resembling the observed shapes of Atlas and Pan. Another frequent type of resulting structures is elongated shapes with characteristics similar to Prometheus, which result from impact parameters close to the boundary between merging and merge-and-split collisions.

Several populations of similar-sized precursors were run with different distributions of initial eccentricities that were derived from the first steps of the study. Depending on the distribution, 20 to 50% of the systems result in flat or elongated moons. These results are consistent with the fraction of small moons possessing peculiar shapes: Pan, Atlas and Prometheus exhibit such features. The remaining of the systems underwent too many hit-and-run collision, that we assume lead to a phase of splat-like merging and re-accretion of ejecta, resulting in a randomized shape within the Roche lobe of the moonlet, as it is the case for Pandora, Janus and Epimetheus.

Acknowledgements

The authors acknowledge support from the Swiss NCCR PlanetS and the Swiss National Science Foundation.

References

- [1] Goldreich, P. & Tremaine, S. Disk-satellite interactions. *Astrophys. J.* **241**, 425-441 (1980).
- [2] Charnoz, S., Salomon, J. & Crida, A., The recent formation of Saturn's moonlets from viscous spreading of the main rings. *Nature* **465**, 752-754 (2010).
- [3] Crida, A. & Charnoz, S., Formation of Regular Satellites from Ancient Massive Rings in the Solar System. *Science* **338**, 1196 (2012).
- [4] Porco, C. C., Thomas, P. C., Weiss, J. W. & Richardson, D. C. Saturn's Small Inner Satellites: Clues to Their Origins. *Science* **318**, 1602 (2007).
- [5] Karjalainen, R., Aggregate impacts in Saturn's rings. *Icarus* **189**, 523-537 (2007).

Saturn's decisive role in the formation of the Galilean system

Thomas Ronnet (1), Olivier Mouis (1), Pierre Vernazza (1), Jonathan I. Lunine (2) and Aurélien Crida (3),(4)

(1) Laboratoire d'Astrophysique de Marseille, Aix Marseille Univ, CNRS, CNES, LAM, Marseille, France

(thomas.ronnet@lam.fr), (2) Department of Astronomy and Carl Sagan Institute, Cornell University, Ithaca, NY 14853, USA,

(3) Université Côte d'Azur/Observatoire de la Côte d'Azur, Laboratoire Lagrange (UMR7293), Boulevard de l'Observatoire, CS 34229, 06300 Nice, France, (4) Institut Universitaire de France, 103 Boulevard Saint-Michel, 75005 Paris, France

Abstract

The four massive Galilean satellites are believed to have formed within a circumplanetary disk during the last stages of Jupiter's formation. However, no consensus exists regarding the origin and delivery mechanisms of the building blocks of the forming satellites. The opening of a gap in the circumsolar disk should have indeed efficiently isolated Jupiter from the main sources of solid material. However, a reservoir of planetesimals should have existed at the outer edge of Jupiter's gap, where solids were trapped and accumulated over time. Here we show that the formation of Saturn's core within this reservoir, or its prompt inward migration, allows planetesimals to be redistributed from this reservoir towards Jupiter and the inner Solar System, thereby providing enough material to form the Galilean satellites and to populate the Main Belt with primitive asteroids. We find that the orbit of planetesimals captured within the circumjovian disk are circularized through friction with gas in a compact system comparable with the current radial extent of the Galilean satellites. The decisive role of Saturn in the delivery mechanism has strong implications for the occurrence of massive moons around extrasolar giant planets as they would preferentially form around planets within multiple planet systems.

1. Context

The Galilean satellites orbiting around Jupiter are generally seen as a by-product of the giant planet's formation. They are believed to accrete in a circumjovian disk during the final stages of Jupiter's own accretion. However, the origin and delivery mechanism of the building blocks of the moons is debated. In fact, the proposed mechanisms, either (1) capture/ablation of large planetesimals in the direct vicinity of Jupiter [1] or (2) delivery of small dust grains entrained with the gas accreted by Jupiter [2], seem incompatible with

the recent developments of the theory of giant planets formation. At the time when satellites supposedly formed, Jupiter should have carved a deep gap in the circum-solar disk whose outer edge acted as a dust trap which would efficiently filtered dust grains, making (2) unlikely to provide enough material to build the moons over time. On the other hand, the formation of planetesimals require specific conditions [3] which were very unlikely met in the direct vicinity of Jupiter whereas already formed planetesimals would have been quickly scattered away by gravitational interactions with the forming giant, leaving Jupiter's vicinity empty by the time the satellites should form.

The dust trap located at the outer edge of Jupiter's gap provides suitable conditions for the formation of planetesimals. Dust grains would accumulate there over time and collapse into larger objects, building-up a reservoir of solid material close to Jupiter. However, these planetesimals would initially reside outside of Jupiter's gravitational reach and a mechanism is needed to deliver them. Here we show that the formation of Saturn would have allowed the delivery of objects to the circumjovian disk. Either Saturn would have formed directly at the outer edge of Jupiter's gap and scattered the planetesimals in its vicinity or it could alternatively have formed further out and migrated inward, thereby pushing material towards Jupiter as its inward 2:1 and 3:2 mean motion resonances swept the reservoir.

2. Results

We conducted N-body simulations including Jupiter, its circum-planetary disk, a circum-solar disk and either a growing (case 1) or migrating Saturn (case 2). Planetesimals were distributed in a narrow annulus at the outer edge of Jupiter's gap and were considered as test particles. The effect of gas drag onto planetesimals (either from the circum-solar or circumjovian disk) was included considering these objects have a

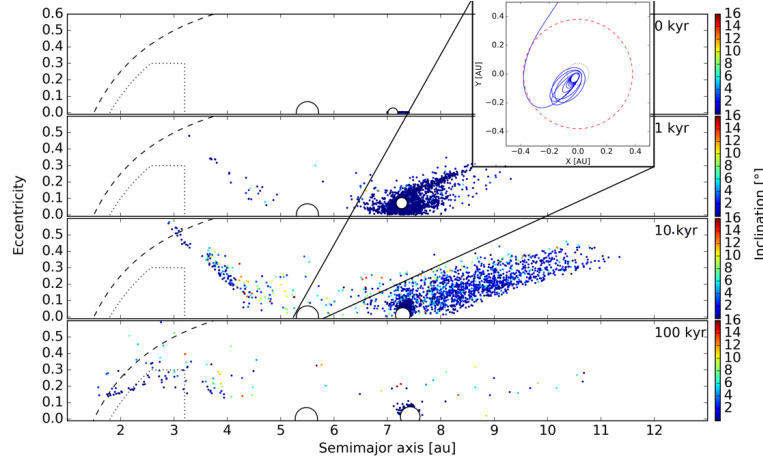


Figure 1: Snapshots of the evolution of planetesimals in a simulation where Saturn is growing at the outer edge of Jupiter’s gap. The dotted box shows the extension of the main asteroid belt and the dashed line shows orbits with perihelion $q < 1.5$ au (i.e., orbits that cross the region of terrestrial planets’ embryos). The box in the upper right part shows an example of orbital evolution of a captured objects in a XY plane centered on Jupiter. The red dashed circle is Jupiter’s Hill sphere and the black dotted circle is the extension of the circum-jovian disk.

radius of 100 km. Planetesimals were considered captured and removed from the simulations if they were found on a bound orbit with respect to Jupiter with a semimajor axis $\leq 0.2 R_H$, where R_H is Jupiter’s Hill radius.

Figure 1 shows the evolution of the system in a case 1 scenario. Saturn’s growth allows an efficient redistribution of the planetesimals, a fraction of which are captured within the circum-jovian disk through gas drag (upper right box shows an example of a prograde capture around Jupiter) while some objects are scattered toward the inner Solar System. For both cases 1 and 2, we find that $\sim 10\text{--}15\%$ of the planetesimals end up captured by Jupiter, with roughly equivalent amount of prograde and retrograde objects, and $\sim 1\%$ of the planetesimals are implanted in the asteroid belt. Subsequent evolution of captured objects reveal that planetesimals captured on initially retrograde orbits are rapidly lost to Jupiter whereas those captured on prograde orbits are circularized through gas drag in a compact system whose radial extension is comparable to that of the current Galilean system.

3. Conclusion

Our results suggest that the building blocks of the Galilean satellites originated from a reservoir of objects located at the outer edge of Jupiter’s gap. A fraction of these primordial objects are likely still present in today’s asteroid belt. These asteroids are probably

the parent bodies of the carbonaceous meteorites collected on Earth which were early on separated from the non carbonaceous parent bodies by Jupiter [4]. The decisive role played by Saturn implies that analogues to the Galilean moons in extrasolar systems would mainly, if not only, form around giant planets within multiple planet systems.

Acknowledgments

P.V. and O.M. acknowledge support from CNES. This work has been partly carried out thanks to the support of the A*MIDEX project (n° ANR-11-IDEX-0001-02) funded by the “Investissements d’Avenir” French Government program, managed by the French National Research Agency (ANR).

References

- [1] Mosqueira, I., & Estrada, P. R. 2003a, *Icar*, 163, 198
- [2] Canup, R. M., & Ward, W. R. 2002, *AJ*, 124, 3404
- [3] Johansen, A., Blum, J., Tanaka, H., et al. 2014, in *Protostars and Planets VI*, ed. H. Beuther et al. (Tucson, AZ: Univ. Arizona Press), 547
- [4] Kruijer, T. S., Burkhardt, C., Budde, G., & Kleine, T. 2017, *PNAS*, 114, 6712

Retrieval of surface spectra in region around Titan's polar lakes

Maëlie Coutelier, Daniel Cordier and Pascal Rannou

Groupe de Spectroscopie Moléculaire Atmosphérique, Université de Reims Champagne-Ardenne, CNRS, Reims, France
(maelie.coutelier@univ-reims.fr)

Abstract

Titan, the largest satellite of Saturn, is surrounded by a very dense atmosphere. The pressure and temperatures allow liquid methane and ethane at the surface. Indeed, the *Cassini/Huygens* mission discovered lakes and seas in the polar regions. The Visual and Infrared Mapping Spectrometer (VIMS) from the Cassini spacecraft took hyperspectral images of Titan. Due to the strong absorption of the methane in the atmosphere, the surface can only be seen in 7 spectral windows centered at 0.93, 1.08, 1.27, 1.59, 2.01, 2.7-2.8 and 5 μm . In this work, we use a radiative transfer model to retrieve the surface albedo of Titan's polar lakes from VIMS spectral images.

1. Introduction

Titan's atmosphere is composed of gases, clouds, and a thick layer of haze. Titan possesses a methane cycle. Like on Earth, there is rain, evaporation, and liquid at the surface. However, the haze surrounding Titan scatters most of the visible light, and the strong absorptions of methane block most of the reflected light on VIMS infrared spectral range. Due to Titan's great distance from the Sun, the light received is weak, so the signal/noise ratio of VIMS data is low. Furthermore, VIMS has a spatial resolution of tens of km. In spite of those disadvantages, the surface geology can be studied in some of VIMS spectral windows. Lakes and seas have been detected on Titan's polar regions by RADAR images. An uncertainty exists about their chemistry : the lakes are estimated to be a mixture of liquid CH_4 , C_2H_6 and other minor species, with dissolved N_2 , and sedimented aerosols. Thermodynamic and experimental constraints have been established for the composition of Titan's lakes [6], but the ratio is still uncertain. The interest of this study is to better determine the composition of the lakes, seas and shores with an inversion of the surface albedo thank to a radiative transfer (RT) model. As the surface albedo

is dependent of the chemical composition, once we have the albedo of the lakes and the areas around, we can compare it to experimental data to determine their compositions[3][6].

2. Objectives of the work

There are traces of evaporites on Titan, especially around the lakes, past and present[1][7][2]. One of the objectives is to study the evaporite albedo with the RT model. First, we retrieve the surface albedo around and on the lakes in order to calibrate the model with a surface albedo assumed to be null [5]. Then, we identify spectral features of the evaporites by detecting eventual differences or variations in the spectra. Finally, we look for particular signatures that could identify the zones around the lakes, like in fig. 1. The lake area is distinct from the circumlacustrine zone.

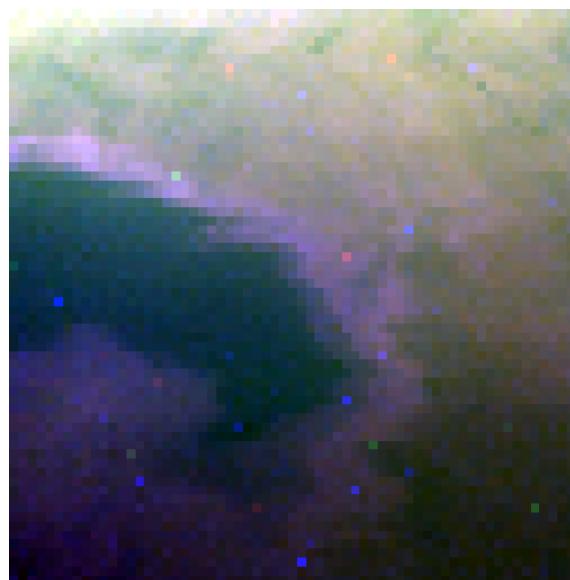


Figure 1: Ontario Lacus, from the VIMS cub V1616820684. RGB channels at 2.03, 1.58 and 2.79 μm . Noise can be seen on the bright-colored pixels.

3. Radiative Transfer Model

The model use the existing solver SHDOMPP developed by K. Evans to solve the RT equations in a plane-parallel approximation. The atmosphere optical properties - such as the single scattering albedo, the phase function, and the optical depth - are determined by using the HASI data for the CH_4 mixing ratio and temperature and pressure profile, Doose's haze extinction coefficient profile, and CIRS data to reproduce the CO, HCN and C_2H_2 vertical profile. We use a correlated-k approximation to calculate the optical depth of the different gases. The spectral rays of the gases (HITRAN database) are used to calculate the absorption coefficients. We used a model of scattering by fractal aggregates to model the haze spectral properties and we used Tomasko's phase functions, adapted according Doose et al. 2016 suggestions [4][8].

4. Comparisons

Using the VIMS pixel's navigation data, we get the incidence, emission and phase angles that we will use in the model to compare the simulated spectra with the spectra of the different pixels. An error minimization routine makes it possible to fit the surface albedo parameter of the model to the pixel's spectra. In this way, we obtain the surface albedo in the spectral windows. Not all the windows can be used, because some parameters are not well defined and that could be improved in the model. For example the C_2H_6 absorptions are not known. The haze vertical profile is not well defined at high latitudes neither. Once cleared of these uncertainties, the surface albedo obtained can be a reliable source to study the surface composition. In figure 2 the result of the model is close to the data, because the latitude is low, and well corresponds to the haze profile.

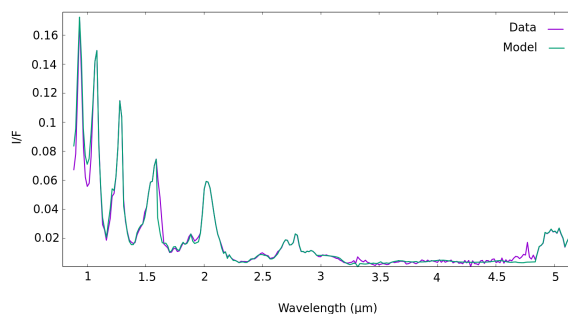


Figure 2: Test of the model, with the pixel (24,34) from the cube C1477457253.

Acknowledgements

The work was founded by the University of Reims Champagne-Ardenne, the Région Grand-Est and the PNP of the CNRS.

References

- [1] Jason W. Barnes, Jacob Bow, Jacob Schwartz, Robert H. Brown, Jason M. Soderblom, Alexander G. Hayes, Graham Vixie, Stéphane Le Mouélic, Sebastien Rodriguez, Christophe Sotin, Ralf Jaumann, Katrin Stephan, Laurence A. Soderblom, Roger N. Clark, Bonnie J. Buratti, Kevin H. Baines, and Philip D. Nicholson. Organic sedimentary deposits in Titan's dry lakebeds: Probable evaporite. *Icarus*, 216(1):136–140, 2011.
- [2] D. Cordier, T. Cornet, J. W. Barnes, S. M. MacKenzie, T. Le Bahers, D. Nna-Mvondo, P. Rannou, and A. G. Ferreira. Structure of Titan's evaporites. *Icarus*, 270:41–56, 2016.
- [3] Daniel Cordier, Olivier Mousis, Jonathan I. Lunine, Panayotis Lavvas, and Véronique Vuitton. Erratum: An estimate of the chemical composition of titan's lakes (Astrophysical Journal Letters (2009) 707 (L128)). *Astrophysical Journal Letters*, 768(1):L23, 2013.
- [4] Lyn R. Doose, Erich Karkoschka, Martin G. Tomasko, and Carrie M. Anderson. Vertical structure and optical properties of Titan's aerosols from radiance measurements made inside and outside the atmosphere. *Icarus*, 270:355–375, 2016.
- [5] Caitlin A. Griffith, Juan M. Lora, Jake Turner, Paulo F. Penteado, Robert H. Brown, Martin G. Tomasko, Lyn Doose, and Charles See. Possible tropical lakes on Titan from observations of dark terrain. *Nature*, 486(7402):237–239, 2012.
- [6] A. Luspai-Kuti, V. F. Chevrier, D. Cordier, E. G. Rivera-Valentin, S. Singh, A. Wagner, and F. C. Wasiak. Experimental constraints on the composition and dynamics of Titan's polar lakes. *Earth and Planetary Science Letters*, 410:75–83, 2015.
- [7] Shannon M. MacKenzie, Jason W. Barnes, Christophe Sotin, Jason M. Soderblom, Stéphane Le Mouélic, Sebastien Rodriguez, Kevin H. Baines, Bonnie J. Buratti, Roger N. Clark, Phillip D. Nicholson, and Thomas B. McCord. Evidence of Titan's climate history from evaporite distribution. *Icarus*, 243:191–207, 2014.
- [8] M. G. Tomasko, L. Doose, S. Engel, L. E. Dafeo, R. West, M. Lemmon, E. Karkoschka, and C. See. A model of Titan's aerosols based on measurements made inside the atmosphere. *Planetary and Space Science*, 56(5):669–707, 2008.

Ground-based Doppler Velocimetry: wind measurements in Saturn's atmosphere with UVES/VLT

M. Silva (1), P. Machado (1), A. Sánchez-Lavega (3), R. Hueso (3), J. Peralta (2) and D. Luz (1)

(1) Institute of Astrophysics and Space Sciences, Observatório Astronómico de Lisboa, Ed. Leste, Tapada da Ajuda 1349-018 Lisboa, Portugal (msilva@oal.ul.pt), (2) Institute of Space and Astronautical Science – Japan Aerospace Exploration Agency (JAXA), Japan, (3) Departamento de Física Aplicada I, E.T.S. de Ingeniería, Universidad del País Vasco, Bilbao, Spain

Abstract

We will present the latest Doppler wind velocity results of Saturn's zonal flow at cloud level. The study of the planet's global system of winds at the 0.7 bar region, promises to improve the characterization of the equatorial jet and the latitudinal variation of the zonal winds, as well the measurement (and monitorization) of its spatial and temporal variability, achieving a better understanding of the dynamics of Saturn's zonal winds (which Sánchez-Lavega [8] have found to have changed strongly in recent years). Finally, the complementarity with Cassini, has provided an independent set of observations to compare with and help validate the method.

1. Introduction

The UVES/VLT instrument has been used, which simultaneously achieves high spectral resolving power and high spatial resolution, with the aperture aligned perpendicularly to Saturn's rotation axis. In this configuration, spatial information in the East-West direction is preserved in a set of spectra in the direction perpendicular to the dispersion. The technique of Absolute Astronomical Accelerometry (AAA) [1] has been applied to the backscattered solar spectrum, to determine the Doppler shift associated with the zonal circulation, retrieved by our measurements in the visible wavelength range of 480-680 nm. Previously we successfully adapted this Doppler velocimetry technique for measuring winds at Venus cloud tops [4] [5] [6]. Since the AAA technique only allows to compare spectra where the line shifts are within the line width, in fast rotating atmospheres (such as Saturn), the spectra must be compared by pairs from adjacent areas of the disk (adjacent pixels in the slit).

2. Observations

The observations consisted of 4 blocks of 15 exposures of 90 seconds, plus two shorter blocks of 9 exposures, totaling 7.3 hours of telescope time. Despite most of the northern hemisphere was covered by the rings, the aperture has been offset by 1 arcsec in the North-South direction (beginning at the South pole) between consecutive exposures. Saturn's diameter was 17.4 arcsec and the slit aperture was 0.3 x 25 arcsec. The sub-terrestrial point was at -26.1 S. The presence of the rings led to severe order superposition. The dark region between the rings and the disk may not be present, depending on the slit position. On the other hand, defects in the response of the UVES slit in the upper part prevent its use for accurate Doppler measurements such as these. For these reasons, only the central part of the aperture has been considered for the measurements. We obtained the zonal wind as a function of local time for all slit's offset positions, except for the cases with ring overlapping. For that we estimated the ring system keplerian velocity at each pixel position, and then, superposed the planet + rings spectra and adjusted the most spectral lines possible (the residual components were due to planetary contribution, mostly methane and ammonia).

3. Summary and Conclusions

The Doppler velocimetry has proven to be a competitive ground-based method able to derive wind's velocities on Saturn, allowing cross-comparison with cloud-tracked winds from Cassini's ISS images (wavelength bands 752-764 nm and 937-964 nm), and the study of short-term variability. We will separate the spectra planetary contribution from methane (and also ammonia) and study the altitude from its contribution, based on NEMESIS radiative model [10]. Detection of finer latitudinal variations in zonal winds in the future will require precise

modeling (radiative transfer model) of the probed level and an improved treatment of methane/ammonia lines and order superposition effects. Nevertheless, our Doppler velocimetry technique stands out as a promising ground-based method for wind monitoring in the giant planets.

Acknowledgements

This work was supported by ULisboa (BD2016), based on the Regulation of Research Fellowships of the University of Lisbon, office n.º 6977/2015, and the Statue of the Research Fellow.

References

- [1] Connes, P. 1985, Absolute astronomical accelerometry, *Astrop. Sp. Sci.*, 110, 211-255.
- [2] García-Melendo et al., 2012, Non-linear simulations of Saturn's 2010 Great White Spot, European Planetary Science Congress 2012, id. EPSC2012-298.
- [3] Luz D. et al., 2006, *J. Geophysics. Res. Planets* 111, E08S90.
- [4] Machado P. et al., 2012, *Icarus*, 221, 248-261.
- [5] Machado P. et al., 2014, *Icarus*, 243, 249-263.
- [6] Machado P. et al., 2017, *Icarus*, 285, 8-26.
- [7] Peralta, J., Sánchez-Lavega, A., Valverde, D., Luz, D., Machado, P., 2015, GRL.
- [8] Sánchez-Lavega, A., et al., 2003, A strong decrease in Saturn's equatorial jet at cloud level, *Nature*, 423, 623-625.
- [9] Widemann, T., Lellouch, E., Donati, J.-F., 2008, *Planet. Sp. Sci.*, 56, 1320-1334.
- [10] Barstow, J. K.; Irwin, P. G. J.; Fletcher, L. N.; Giles, R. S.; Merlet, C. 2006, *Icarus*, 271, 400-417

Giant Impacts Around Saturn

Erik Asphaug and Alexandre Emsenhuber

University of Arizona, Lunar and Planetary Laboratory, Tucson, Arizona, United States (asphaug@lpl.arizona.edu)

Abstract

We revisit a scenario for the formation of Saturn's middle-sized moons. Saturn would begin with a Jupiter-like system of 'galilean' moons that underwent dynamical collapse, with the collisional mergers ultimately forming Titan. The middle-sized moons formed by the release of ice-rich material in the spiral arms that form in the immediate aftermath of the collisions. We aim at improving the realism of similar-sized collisions in the vicinity of another massive body by including the tidal forces in the collision simulation. This puts a constraint on the location where the impact occurred. Moreover, the inclusion of friction influences the formation of the spiral arms, and the sizes and morphologies of clumps.

1. Background

The origin of the Saturnian satellites is an evolving mystery. Titan, orbiting at $a = 20.3 R_H$, is about equal in mass to all the satellites of Jupiter combined, when normalized to the planet's mass. The origin and evolution of its high orbital eccentricity ($e = 0.0288$) is a classic problem in planetary science, as is its remarkably active geology compared to Ganymede and Callisto, two jovian satellites of approximately the same size and density, especially the existence of an almost Earthlike atmospheric/cryo-hydrologic cycle. Titan's periapsis is closer to Saturn than its apoapsis by $1.2 R_H$, causing a strong non-equilibrium tide; in the absence of forcing, Titan's orbit should have circularized within a few billion years [6] due to the dissipation of tidal energy. It would appear that either Titan was formed with significantly greater eccentricity than it has today, or its orbital eccentricity has been acquired more recently or is forced, with no obvious options for either (see however [2]).

The middle-sized moons (Mimas, Enceladus, Tethys, Dione, Rhea, Hyperion, Iapetus) are a connected mystery, beginning with their extraordinary compositional diversity. Radar observations [5] reveal considerable variations in their near-surface proper-

ties. Compositionally and geologically they are highly diverse. Innermost Mimas, 400 km diameter, is an inactive world of mostly ice ($\rho = 1.15 \text{ g/cm}^3$), but its neighbor Enceladus (500 km diameter) is about half rock (1.61 g/cm^3) and is one of the most active satellites in the Solar System. Tethys (0.98 g/cm^3) and Mimas, the ice-dominated inner MSMs, are in a 2:1 mean motion orbital resonance, and so are the two rockiest, Enceladus and Dione ($\rho = 1.43 \text{ g/cm}^3$). To add to the complexity of the system, Tethys and Dione are the only moons in the Solar System to have co-orbital satellites at their Lagrange points, and Hyperion is in 4:3 mean motion resonance with Titan. And to round out the picture, the two largest (Rhea, 1.24 g/cm^3 , and Dione) are of average bulk composition, while the three smallest, Mimas, Enceladus and Hyperion, could hardly be more dissimilar.

To address these two issues, the unique characteristics of Titan and the diversity of the middle-sized moons (MSMs), Asphaug and Reufer (2013) [1] developed a scenario where Saturn began with a 'galilean' system of moons comparable to Jupiter's, that underwent dynamical collapse, with collisional mergers ultimately forming Titan. The collisional accretion of Titan through a series of giant impacts has the benefit of leaving behind a finished satellite with substantial eccentricity (~ 0.1) that would decrease with tidal evolution. Moreover the frictional and accretionary (gravitational binding) energy released in the merger might explain the geological uniqueness of this large moon. Mergers liberate ice-rich spiral arms around the merged body in their simulations; these self-gravitate into escaping clumps resembling MSMs in size and compositional diversity. [1] reasoned that MSMs were spawned in a series of giant collisional mergers around Saturn, while Jupiter's original satellites stayed locked in resonance. They considered various causes for the dynamical collapse, but focused mainly on the clump-producing SPH simulations of these collisions, that are capable of producing tens of clumps, fragments from each merger that maintained unique identities as satellites around Saturn for some time. An open question is whether these

satellites, which in SPH simulations have characteristics that are surprisingly comparable to the MSMs in size and compositional diversity, can survive to long time and avoid ultimately being accreted by the larger bodies in the system. If dozens of clumps were produced by this series of mergers, then a fraction of those clumps must survive. To study that aspect of the problem requires attention to the realism of similar-sized collisions and mergers and attempted mergers when the colliding bodies are in the strong gravitational influence of a central planet.

2. Giant impacts around a central body

We begin with the basic problem of improving the realism of the giant impacts. To our knowledge there are no studies of the physics of giant impacts happening well inside of a central body's gravitational field, so we are performing suites of simulations to reproduce the simulations of [1] but at various radii from Saturn. The threshold for clumps escaping from a given merger is lower, so that more MSMs will be produced. But also, the dynamics of a graze and merge collision are transformed considerably, in our pilot calculations, so that what would be a graze and merge collisions becomes a hit and run, and what may be a simple accretion becoming graze and merge, or a so-called hit and run return [3].

Moreover, the proposed satellite-forming giant impacts would have occurred well inside the regime where friction will matter during giant impacts [4]. So we have explicitly included the influence of solid friction in our studies, which may strongly influence the dynamics leading to clump formation. It should be noted that the proposed collisional mergers, at or around the escape velocity of Titan, ~ 2 km/s, are overall subsonic so that there will be little or no shock melting, although there may be considerable frictional heating. In this velocity range it appears that the most common outcome is graze and merge, when considering all impact angles. The typical sequence for shallow impacts $\theta > 60^\circ$ involves two to three collisions until the impactor is finally accreted. The first collision captures the impactor, which subsequently ranges to roughly $10 R_S$ before the second collision occurs. The second and third collisions then produce spiral arms, from which the smaller clumps are formed.

The presence the central planet will affect the whole process in two ways: the return trajectory of the impactor and the clump formation in the spiral arms.

With Saturn and Titan's bulk densities, the Hill radius is $R_H = a_S(M_S/3M_T)^{1/3} \sim R_S \cdot a_S/R_T$. In case the collision happens at the current location of Titan, all the collision remain well within the Hill sphere. However if the impact occurred closer in then the distances will become comparable to the Hill radius. To asses the effect of Saturn on the formation of the MSMs, we are including in our simulations an additional force to represent the differential tidal effects of the presence of a third massive body. This adds another layer of complexity to the problem, as now the distance and directions of that body are now parameters. The inclusion of friction also influences the formation of the spiral arms, and the sizes and morphologies of clumps.

To first order, when the 'bouncing' impactor strays beyond the Hill radius in a graze and merge collision, this usually implies its loss, although that limit is not precise. This implies that if the impact takes place closer in than about $10 R_T$, then the impact is not graze and merge, but hit and run. This would prevent the formation of the MSMs with the original scenario, but also, it would leave two projectiles that are likely to collide again sometime in the near future, several thousand orbits later. Before we can further consider the detailed dynamical evolution of this scenario using an N -body formalism, our goal is to obtain a comprehensive understanding of the unique nature of satellite-forming giant impacts.

References

- [1] Asphaug, E. and Reufer, A.: Late origin of the Saturn system. *Icarus*, Vol. 223, pp. 544-565, 2013.
- [2] Čuk, M., Dones, L. and Nesvorný, D.: Dynamical evidence for a late formation of Saturn's moons. *ApJ*, Vol. 820, pp. 97-, 2016.
- [3] Emsenhuber, A. and Asphaug E.: Sequential Giant Impacts. *EPSC Abstracts*, Vol. 12, 2018.
- [4] Emsenhuber A., Jutzi, M. and Benz, W.: Moon-Forming Giant Impacts with Icy Impactors, in revision.
- [5] Ostro, S. J., West, R. D., Wye, L. C., Zebker, H. A., Janssen, M. A., Stiles, B., Kelleher, K., Anderson, Y. Z., Boehmer, R. A., Callahan, P., Gim, Y., Hamilton, G. A., Johnson, W. T. K., Veeramachaneni, C., Lorenz, R. D. and The Cassini Radar Team: New Cassini RADAR results for Saturn's icy satellites. *Icarus*, Vol. 206, pp. 498-506, 2010.
- [6] Tobie, G., Mocquet, A. and Sotin, C.: Tidal dissipation within large icy satellites: Applications to Europa and Titan. *Icarus*, Vol. 177, pp. 534-549, 2005.

Unusual Magnetic Fields of Neptune and Uranus

William Nellis

Department of Physics, Harvard University, USA (nellis@fas.harvard.edu)

Abstract

A large database has been measured for likely fluids in Uranus and Neptune (U/N) at pressures and temperatures up to 180 GPa and a few 1000 K. Those data yield an explanation of why magnetic fields of U/N and Earth are so different. Fields of U/N are made at 90% of their outer radii and thus have non-dipolar contributions. Earth has a strong rotating rock mantle that couples its rotation into its Fe-rich fluid outer core. In contrast Uranus and Neptune have no such mechanism and so magnetic field geometries of U/N are free to wander unconstrained.

1. Introduction

NASA's Voyager 2 spacecraft flew by Uranus and Neptune (U/N) and measured their magnetic and gravitational fields [1]. The gravity data detected two layers in each, a low-density envelop composed mostly of H and He and a high density core [2] composed of planetary "Ice", a fluid mostly of H₂O, NH₃, and CH₄, plus Rock. Magnetic-field intensities of U/N are comparable to Earth's. Spatial dependences of those fields are non-dipolar and non-axisymmetric, unlike Earth's nearly dipolar and nearly axisymmetric magnetic field.

If the measured magnetic fields of U/N are force-fit to dipoles, those effective magnetic axes are tilted 59° and 47° from their respective rotational axes and their effective dipole centers are offset by 33% and 55% of their respective radii. The reason why magnetic fields of Earth and of U/N differ so greatly has been a major unresolved question. The purpose of this paper is to report a model based on experimental data measured on Earth and Voyager 2 observations, which provides a likely explanation of why those planetary field geometries are so different.

2. Basic Ideas

Planetary magnetic fields are made by dynamos: convective paths of electrically conducting fluids across lines of magnetic force. To determine why magnetic fields are as they are, one needs to consider measured electrical conductivities and equations of state of likely constituent fluids at pressures P and temperatures T at which planetary magnetic fields are made and likely coupling mechanisms between layers of materials that might affect convective flows. An extensive experimental database for fluid H₂, O₂, N₂, H₂O, NH₃, CH₄, the "Icy" mixture Synthetic Uranus, CO, CO₂, and several hydrocarbons has been measured up to P and T of 180 GPa (1.8×10^6 bar) and several 1000 K under dynamic compression with experimental lifetimes of 100 ns, more than sufficient to obtain thermal equilibrium in dense fluids [3,4]

Those dynamic compression results were measured at Lawrence Livermore National Laboratory, starting in 1980 when Voyager 2 headed for U/N on departing Saturn. Extreme P/T s were generated by impact at velocities up to 7 km/s generated with a two-stage gas gun. Liquid samples were contained in small cryostats at 20 K for liquid H₂, for example. Measured electrical conductivities indicate fluid H is semiconducting from 93 to 140 GPa and a poor metal from 140 to 180 GPa with electrical conductivity of 2000/(ohm-cm). Corresponding calculated T s range from 1700 to 2600 K at pressures from 93 to 140 GPa and then up to 2900 K at 180 GPa [5]. "Icy" molecules that accrete during formation of U/N decompose at high interior P/T above ~100 GPa.

The facts that the magnetic field of Earth is dipolar and nearly aligned with its axis of rotation and that the magnetic fields of U/N are neither implies that Earth's field is made primarily by convective loops strongly coupled to planetary rotation; the convective loops of U/N are virtually decoupled from planetary rotation. The dipolar field of Earth implies its external magnetic field is made deep in that planet [6]; Fe-rich convecting fluid extends only up to the Core-Mantle Boundary (CMB) at half the outer radius of Earth. Because dense conducting fluid H is

a good electrical conductor above 90 GPa at about 90% the outer radii of U/N, the external magnetic fields of U/N are made relatively close to their outer surfaces. Thus, their magnetic fields are expected to have non-dipolar contributions [6] as observed.

The coupling of Earth's Fe-rich fluid outer core to Earth's rotation has been demonstrated by Hide et al [7]. Small decay of the length of a day over 150 years can be understood by an interaction at the CMB. Earth has a strong, rock mantle that rotates at nearly constant angular velocity, which is expected to form current loops in convecting Fe-rich fluid such that Earth's magnetization is generated to nearly align itself along its rotational axis. Several possible interactions might cause coupling between Earth's strong, rock mantle across its relatively sharp CMB, one of which is an estimated surface roughness of less than 0.5 km on the inner radius of the Earth's mantle (3500 km) [7].

Tendency for Earth's magnetic field to orient along its axis of rotation derives from the fact that potential energy of interaction between magnetization M produced by current flowing in a loop in an external magnetic field B is minimized when M and B point in the same direction. For a spherical ensemble of convective loops rotating at constant angular velocity about an axis of rotation, magnetic field at any one loop is the vector sum of magnetic fields produced by all the other convective loops.

U/N have weak fluid H-He envelopes and weak fluid cores. In this case convective dynamo motions are expected to be weakly coupled to global rotational motions of U/N. Thus, the dynamos of U/N would be relatively free to wander as local conditions dictate. In this case effective tilt angles and effective center-offsets of their magnetic fields would be expected to vary slowly and unconstrained over the age of the Solar System. "Polar wander" is a good descriptor for the time dependence of magnetic fields of U/N.

3. Summary and Conclusions

Based on a substantial database measured over three decades for numerous representative planetary fluids at high P/T generated with a two-stage light-gas gun, the non-dipolar non-axisymmetric magnetic fields of Uranus and Neptune are (i) made primarily by degenerate metallic fluid H (MFH) at or near crossovers from H-He envelopes to "Ice" cores at ~ 100 GPa (Mbar) pressures and $\sim 90\%$ the radii of

U/N; (ii) numerous likely planetary fluids investigated experimentally decompose at P/T above ~ 100 GPa or less and few 1000 K; (iii) thus there probably is little molecular nebular "Ice" in the Ice Giants; (iv) electrical conductivity of MFH is up to a factor of 100 larger than conductivity of "Ices" thought previously to make the magnetic fields of U/N (20/(ohm-cm) [8]); (v) because those magnetic fields are made close to outer surfaces, non-dipolar magnetic fields can be expected as observed; (vi) "Ice" cores are a heterogeneous mixture of nebular Ice and Rock that accreted, sank below the H-He envelopes into the cores in which nebular materials decomposed at high P/T and probably re-reacted to form new chemical species; (vii) those magnetic fields are probably non-axisymmetric because rotational motions of U/N are weakly coupled to convective motions that make their magnetic fields. For U/N "polar wander" is a good descriptor for variations of magnetic field over time.

References

- [1] U. S. National Aeronautics and Space Agency Voyager Program website.
- [2] R. Helled, J. D. Anderson, M. Podolak, and G. Schubert: Interior models of Uranus and Neptune, *Astrophysical Journal*, Vol. 726, pp. 15-1-15-7, 2011.
- [3] W. J. Nellis: The Unusual Magnetic Fields of Uranus and Neptune, *Modern Physics Letters B*, Vol. 29, pp. 1430018-1-1430018-29, 2015.
- [4] W. J. Nellis: *Ultracondensed Matter by Dynamic Compression*, Cambridge University Press, 2017.
- [5] W. J. Nellis, S. T. Weir, and A. C. Mitchell: Minimum Metallic Conductivity of Fluid Hydrogen at 140 GPa (1.4 Mbar), *Physical Review B*, Vol. 59, pp. 3434-3439, 1999.
- [6] K. D. Granzow: Spherical Harmonic Representation of the Magnetic Field in the Presence of a Current Density, *Geophysical Journal of the Royal Astronomical Society*, Vol. 74, pp.489-505, 1983.
- [7] R. Hide, R. W. Clayton, B. H. Hager, M. A. Spieth and C. V. Voorhies: Topographic Core-Mantle Coupling and Fluctuations in the Earth's Rotation. In *Relating Geophysical Structures and Processes: The Jeffrey Volume*, *Geophysical Monograph* 76, Vol. 16, eds. K. Aki and R. Dmowska, IUGG, pp. 107-120, 2013.
- [8] W. J. Nellis et al: The Nature of the Interior of Uranus Based on Studies of Planetary Ices at High Dynamic Pressure, *Science*, Vol. 240, pp. 779-781, 1988.

Exploring the atmosphere of Jupiter with ultraviolet spectroscopy

Henrik Melin (1), L. N. Fletcher (1), A. Antunano Martin (1), J. S. D. Blake (1), P. T. Donnelly (1), N. Rowe-Gurney (1).
(1) University of Leicester, Department of Physics & Astronomy, Leicester, UK,

Abstract

By analysing spectral emission and absorption features over a range of wavelengths emanating from Jupiter's troposphere and stratosphere, we can retrieve the density and temperature of the constituents within it. Here, we present an analysis of Cassini UVIS far-ultraviolet observations of Jupiter, obtained in late 2000. These show the belt and zone structure present in the reflectance spectra long-ward of 160 nm, a region that shows absorption by acetylene and ammonia. We have compiled the relevant cross sections and have integrated these into the NEMESIS radiative transfer and atmospheric retrieval algorithm code. Using this tool, we have performed a search and sensitivity test, identifying the absorption features present in the observed spectrum, retrieving zonally averaged meridional profiles of acetylene and ammonia for comparison with similar results from the Cassini/CIRS investigations (Nixon et al., 2010; Achterberg et al. 2006, Fletcher et al., 2009) at mid-infrared wavelengths. Having developed the tool required to retrieve atmospheric abundances from ultraviolet spectra, we outline its applicability to future ultraviolet observations at Jupiter by ESA JUICE.

Exploring Titan's Meteorology with Dragonfly

S. C. R. Rafkin(1), R. D. Lorenz(2), E. P. Turtle(2), J. W. Barnes(3), M. G. Trainer(4), A. Le Gall(5), J. M. Lora(6), C. P. McKay(7), C. E. Newman(8), M. P. Panning(9), T. Tokano(10), C. Wilson(11) and the Dragonfly Science Team.

(1)Southwest Research Inst., Boulder, CO (rafkin.swri@gmail.com), (2)Johns Hopkins Applied Physics Lab., Laurel, MD, (3)Univ. Idaho, Moscow, ID, (4)NASA Goddard Space Flight Center, Greenbelt, MD, (5)Laboratoire Atmosphères, Milieux, Observations Spatiales, Guyancourt, France, (6)Univ. California, Los Angeles, CA, (7)NASA Ames Research Center, Moffett Field, CA, (8)Aeolis Research, Pasadena, CA, (9)Jet Propulsion Laboratory California Institute of Technology, Pasadena, CA, (10)Inst. für Geophysik und Meteorologie, Univ. Köln, Köln, Germany, (11)Oxford Univ., Oxford, UK

Abstract

Dragonfly [1] is a rotorcraft lander mission (Fig. 1) currently in a Phase A study under NASA's New Frontiers Program that would take advantage of Titan's dense atmosphere and low gravity to visit a number of surface locations, studying how far chemistry can progress in environments that provide key ingredients for life. This mission architecture also permits and demands investigation of Titan's atmosphere.

If selected for flight *Dragonfly* will launch in 2025 and arrive in 2034. It will spend over two Earth years on Titan's surface, long enough to observe many diurnal cycles, atmospheric waves, and perhaps even seasonal changes. *Dragonfly* will explore the meteorology of a number of different locations and terrains, and take vertical profiles of temperature, methane, and hydrogen to constrain diurnal mixing in the planetary boundary layer (PBL).

Dragonfly will also contribute to atmospheric science by measuring surface properties, including soil moisture, conductivity and thermal inertia, the chemical composition of surface deposits (which may contain the products of high-altitude photochemistry), the saltation threshold of Titan's dune particles (which will aid interpretation of dune morphology), and the possible confirmation of fluvial sediments (which may inform our understanding of the hydrologic cycle). *Dragonfly* results will test and improve atmospheric models, enabling a deeper understanding of both the local and global Titan climate system.

1. Instrumentation and Operations

Proposed Titan science operations feature dozens of flights over the mission, although most of the time (~99%) will be spent on the surface. In addition to cameras and chemistry/astrobiology instrumentation, *Dragonfly* includes a Geophysics and Meteorology package ("DraGMet"). This includes optical sensing of methane humidity; a solid-state hydrogen abundance sensor; pressure and temperature sensors; and wind sensors derived from those flown on Beagle 2 mounted on each rotor hub so that one is always upwind of the vehicle to avoid wake effects. Winds aloft will be determined from the vehicle navigation system during flight. DraGMet also incorporates sensing of the electric field and dielectric constant to measure surface properties and the Schumann resonance, plus instrumentation to measure seismic and surface thermal properties. A camera suite will acquire panoramic imaging that will be used to infer atmospheric opacity and some cloud properties.

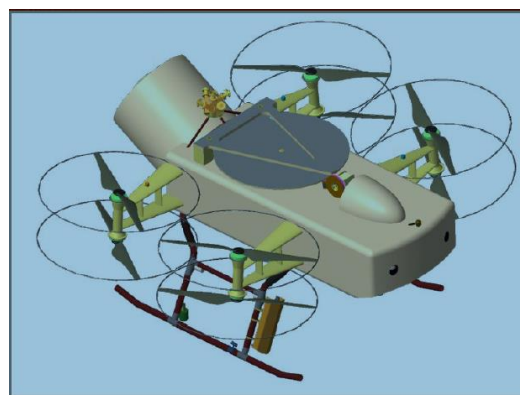


Figure 1: A conceptual CAD model of the *Dragonfly* rotorcraft.

2. Meteorological Science

Titan's meteorology, with a methane-based hydrologic cycle analogous to our own demands study not only in its own right, but as context for the distribution of surface materials, many of which are of astrobiological interest. Measurements of temperature, pressure, winds and methane abundance, both at the surface and during flight, will address key questions about the structure and dynamics of the atmosphere, as well as its exchange of mass, momentum and energy with the surface.

2.1 Surface Meteorology

Dragonfly will make measurements of the meteorological diurnal cycle on Titan, addressing such questions as: How does surface moisture influence temperature? How strongly are winds controlled by local topography (including dunes) versus the global circulation or regional slope winds? Can a gravitational tide component to Titan's winds be isolated? What is the diurnal and synoptic variability of pressure, temperature, and winds? Is there evidence of the intertropical convergence zone in pressure, winds or humidity? Is there evidence of mesoscale to large-scale wave activity at the surface? Are surface temperature variations ~1K, as suggested from Cassini measurements and atmospheric models, or are there larger variations at the small scale on low-albedo, low thermal inertia surfaces such as dunes?

2.2 Vertical Structure

Dragonfly will determine the depth of the PBL and identify structures associated with residual boundary layers, and address such questions as: How representative is the Huygens descent profile (currently the only detailed measurement of the structure of the lower atmosphere)? Are changes in stability associated with the top of the PBL from prior seasons? Is there horizontal spatial variability in the PBL structure? What is the vertical profile of wind and how does it change with location and time?

2.3 Aeolian Activity

Dragonfly will measure the saltation threshold by using its rotors at low power settings to apply increasing wind stress to the surface (e.g. of a dune) until sediment transport begins. Atmospheric models will be constrained using measurements of winds,

and characterization of dunes will then be used to address: Is dune morphology and orientation consistent with present-day winds predicted in circulation models (and if so, with what saltation threshold?) or is there a paleoclimate signal in the dune configuration?

2.4 Methane Cycle and Hydrogen Profile

Dragonfly will quantify the abundance of CH₄ and H₂ and will connect surface abundance and variability to observed vertical profiles, addressing questions such as: How is methane distributed in the vertical? Is the Huygens profile typical? Is there fog or clouds? Is there a surface hydrogen sink? Are there horizontal variations in methane (e.g. associated with soil moisture, springs)? How does humidity vary with the diurnal cycle? Is moisture fluxed out of the ground during the day and returned during the night? Is there a preferred direction of atmospheric moisture transport during this season? Are methane cloud systems visible?

References

[1] Lorenz, R. et al., *Dragonfly : A Rotorcraft Lander Concept for Scientific Exploration at Titan*, Johns Hopkins Technical Digest, in press (2018). Downloadable at <http://dragonfly.jhuapl.edu/>

Investigating the surface distribution of N₂, CH₄ and CO ices on Triton with a volatile transport model

Tanguy Bertrand (1,2), François Forget (2), Bruno Sicardy (3), Emmanuel Lellouch (3)

(1) NASA Ames Research Center, Moffett Field, CA 94035, USA (2) Laboratoire de Météorologie Dynamique, IPSL, Sorbonne Universités, UPMC Univ Paris 06, CNRS, 4 place Jussieu, 75005 Paris, France (3) LESIA-Observatoire de Paris, CNRS, UPMC Univ Paris 06, Univ. Denis Diderot, Sorbonne Paris Cité (tanguy.bertrand@nasa.gov).

1. Introduction

The flyby of Pluto by New Horizons in July 2015 highlighted the extraordinary complexity of the main icy bodies of the Kuiper Belt. The largest satellite of Neptune, Triton, is thought to belong to this family and is often referred as the twin sister of Pluto, as both bodies share similar sizes, densities, atmospheric composition, pressures and temperatures, types of ices (water ice, and volatile nitrogen, methane, CO ices) and probably comparable climate and geology (in particular that related to the flow of nitrogen ice and the condensation-sublimation cycles). However, Triton developed a different (and maybe even more complex) personality than its sister, as attested for instance by the observation of active geysers by Voyager 2 during the 1989 flyby or by the much higher surface albedo (suggestive of extensive resurfacing). In addition to the Voyager data, several ground-based observations of Triton's as well as modeling effort have been performed, leading to different scenarios for the surface distribution of the volatile and non-volatile ices [1][2][3].

Here we present numerical simulations designed to model the evolution of Triton's volatiles over millions of years on the basis of straightforward universal physical equations.

The model used is derived from the Pluto volatile transport model [4], in which the characteristics of Triton's orbit have been used. Our main goal is to investigate where the volatile ices tend to accumulate on Triton, and compare our results with the available observation in order to paint a global portrait of Triton's face. In particular, we investigate if a perennial northern polar cap of nitrogen ice can form.

2. The volatile transport model

1.1 A common model for Pluto and Triton

The model is derived from the Pluto volatile transport model, and takes into account the volatile cycles of N₂, CH₄ and CO [4], a glacial flow scheme for N₂ ice [5] and the seasonal variation of the subsolar point specific to Triton. This variation is complex and we used the solution from [6], which we extrapolated to simulate Triton over the last millions of Earth years.

As in the Pluto model, we consider that Triton's atmosphere is very thin and almost transparent so that it has a negligible influence on the surface thermal balance. We parametrize the atmospheric transport using a characteristic time for the redistribution of the surface pressure and trace species, based on reference GCM simulation.

1.2 Sensitivity parameters

As it is the case for Pluto, the modeled ice cycles on Triton are sensitive to the assumed surface and subsurface properties, which are poorly constrained for now. The key parameters of the model are:

- The ices albedo and emissivity, which can evolve depending on the age or thickness of the deposits and on the sublimation or condensation flux.
- The thermal inertia for each ice, and the geothermal flux.
- The reservoir of volatile ices, which is thought to be less than on Pluto due to the volatile escape following the capture process by Neptune and the subsequent tidal interactions and heating of the surface and escape [7].
- The topography, which likely impacts the volatile ice distribution as it is the case on Pluto.

3. Preliminary results

We investigate the presence and stability over time of a northern polar cap of nitrogen, assuming that there is a perennial cap at the south pole. We show a brief example of simulation.

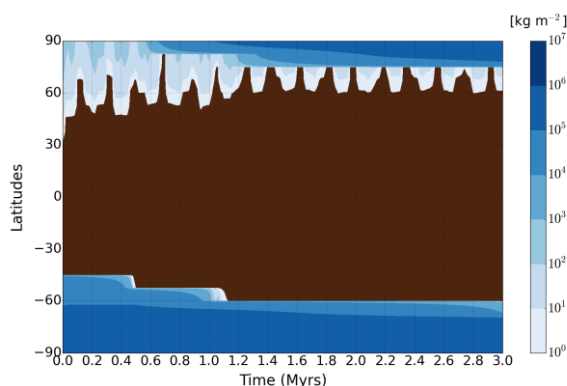
3.1 Initial state of the simulation

We place a 100 m N_2 ice deposit below $50^\circ S$. N_2 ice has an albedo of 0.7 in the model, an emissivity of 0.8 and a thermal inertia of 800 SI. The rest of the surface is volatile-free and has a very dark albedo of 0.1, coupled to a high soil thermal inertia of 1000 SI. The soil temperatures are initialized at 50K.

3.2 Volatile evolution

As shown by Figure 1, we obtain a slight retreat of the initial south polar cap and the formation of a perennial polar cap above $75^\circ N$. N_2 frosts form between $60^\circ N$ - $75^\circ N$.

Figure 1: Simulated evolution of the amount of N_2 ice over 3 million years. The dark brown color indicates the volatile-free regions.



3.3 Discussion

In most of our simulation performed, a perennial polar cap of nitrogen forms in the northern hemisphere. It may not form only if we assume a very high thermal inertia (>2000 SI) coupled to a low bedrock surface albedo (<0.1) and a not too large reservoir for the south polar cap (<2 km). However, Triton's surface is very bright and such a low albedo does not seem realistic. Consequently, our results support the presence of a north polar cap of nitrogen ice.

We plan to further explore the impact of each key parameter on the results. In particular, an asymmetry of topography or geothermal flux may favor one cap over the other. In addition, we will compare the model results with the available observations of Triton. In particular, we aim to reconcile a consistent pressure cycle and methane and CO atmospheric mixing ratio with an extension of the south polar cap in accordance with Voyager 2's observations.

Acknowledgements

T. B. was supported for this research by an appointment to the National Aeronautics and Space Administration (NASA) Post-doctoral Program at the Ames Research Center administered by Universities Space Research Association (USRA) through a contract with NASA.

References

- [1] Holler, B. J. et al.: On the surface composition of Triton's southern latitudes, *Icarus*, 267:255, 2016.
- [2] Spencer, J. R. and Moore, J. M.: The influence of thermal inertia on temperatures and frost stability on Triton, *Icarus*, 99:261, 1992.
- [3] Grundy, W. M. et al.: Near-infrared spectral monitoring of Triton with IRTF/SpeX II: Spatial distribution and evolution of ices, *Icarus*, 2:594, 2010.
- [4] Bertrand, T. and Forget, F.: Observed glacier and volatile distribution on Pluto from atmosphere-topography processes, *Nature*, 987:42, 2016.
- [5] Bertrand, T., et al.: The nitrogen cycles on Pluto over seasonal and astronomical timescales, *Icarus*, 309:277, 2018.
- [6] Forget, F., et al.: A New Model for the Seasonal Evolution of Triton, *DPS* 32, 32:1082, 2000.
- [7] McKinnon, W. B. et al.: Origin and evolution of Triton, In: *Neptune and Triton*, University of Arizona Press, Tuscon, pp. 807-877, 1995.

Forced Rotational Oscillations and Tidal Evolution of Close-in Terrestrial Planets and Planetary Satellites

Sylvio Ferraz-Mello, Hugo A. Folonier, Eduardo Andrade-Ines, Gabriel O. Gomes
Insitute of Astronomy, Geophysics and Atmospheric Sciences, University of São Paulo, São Paulo, Brasil (sylvio@usp.br)

Abstract

The creep tide theory [1] and the Maxwell tide model [2] show that the rotation of close-in terrestrial planets and planetary satellites are damped by tidal effects to periodic attractors nearly commensurable with the orbital period (frequency ratios $1/2$, 1 , $3/2$, 2 , $5/2$, ...). They also show that the final solutions are not stationary, but are forced oscillations (physical librations) around one center, even when no permanent triaxiality exists. These forced oscillations affect the evolution of the systems and the dissipation, which may depart from the solutions obtained from classical averaged models. A new model proposed by Folonier et al. [3] allows us to simultaneously calculate the tidal deformations and the body.

dynamics and extension to Mercury and exoplanets host stars" *Celest. Mech. Dyn. Astr.* 122, 359, 2015

[2] Correia, A.M., Boué, G., Laskar, J. and Rodrigues, A. "Deformation and tidal evolution of close-in planets and satellites using a Maxwell viscoelastic rheology", *Astron. Astrophys.* 571, A50, 2014

[3] Folonier, H.A. et al. In preparation

Aknowledgements

Investigation sponsored by the National Council of Scientific Investigations (CNPq) and the São Paulo State Research Foundation (FAPESP) (Brasil).

References

[1] Ferraz-Mello, S. "Tidal synchronization of close-in satellites and exoplanets: II. Spin

Probing the Atmospheres of Saturn and Uranus with Ground-Based Radio Observations

Mark Hofstadter (1), Virgil Adumitroaie (1), Sushil Atreya (2), and Bryan Butler (3)

(1) Jet Propulsion Laboratory, California Institute of Technology, California, USA (mark.hofstadter@jpl.nasa.gov), (2) University of Michigan, Ann Arbor, USA, (3) National Radio Astronomy Observatory, New Mexico, USA

Abstract

We have analyzed observations of Saturn and Uranus at wavelengths from ~1 millimeter to ~1 meter, which probe the atmospheres from pressures near 0.1 bar (the tropopause) down to pressures of 100's of bars. Our results provide new clues about the composition and chemistry of giant planet atmospheres, and highlight differences between gas- and ice-giants.

1. Introduction

The thermal emission of the giant planets at millimeter to meter wavelengths is controlled by the vertical profiles of temperature and composition from mbar to tens of kbar pressures. Typically, temperatures are taken as known because the expected compositional variations have a much larger effect on radio brightness than do the expected temperature variations. We therefore use spacecraft occultation and ground-based infrared measurements to set the stratospheric and tropopause temperatures of the planets, and take the tropospheric temperature profile to be a convective (wet pseudo-adiabatic) profile. This leaves composition as our free parameter. Based on cosmic abundances, the dominant species our microwave data are sensitive to are NH_3 , H_2O , H_2S , and perhaps PH_3 and CO . At meter wavelengths we may probe to depths where we sense free electrons from pressure-induced ionization.

2. New Data, New Models

New Saturn measurements have been made at cm to meter wavelengths using the eVLA, GMRT and LOFAR radio telescopes. The primary purpose of this data set is to try and constrain the water abundance in the deep troposphere. Reduction of the eVLA data is ongoing. It is extremely complicated at

meter wavelengths due to the many background galaxies which emit strongly at low frequencies. Unfortunately, the GMRT data [1] have large error bars, and the LOFAR data in hand may not be usable.

The new Uranus measurements we are analyzing are unpublished observations at submillimeter to 20 cm wavelengths, all collected near 2006.

From the data sets, we retrieve gas abundances using an optimal estimation technique [2] coupled to a forward model based on [3] but incorporating new laboratory measurements of the microwave opacity of relevant gases which were made in support of the Juno mission to Jupiter [4].

3. Analyses and Work Underway

3.1 Saturn

At Saturn, the currently available microwave data set suggests NH_3 abundances are between about 5 and 10x solar. If NH_3 is as low as 5x solar, the water abundance needs to be at least 10x solar. If the NH_3 abundance is as large as 10x solar, water is poorly constrained by the data set. We hope that the new eVLA data, when reduction is complete, will place tighter constraints on abundances due to smaller error bars, and will allow us to look for temporal variations.

3.2 Uranus

We find that Uranus' deep atmospheric NH_3 abundance is between 0.2 and 0.6x solar, while H_2S is 1 to 2x solar. The submillimeter to millimeter data suggest the presence of an upper tropospheric absorber such as PH_3 at 3x solar. The longest-wavelength Uranus data, at 20 cm, only weakly constrain the deep water abundance, but favor values >3x solar. We are currently working to refine

our forward model (e.g. with newer opacity measurements such as [5] and [6], and hope to explore how chemical processes in the water cloud and interior oceans can explain the low abundances (relative to Solar) of NH_3 and H_2S , and the enhancement of H_2S relative to NH_3 .

4. Discussion

Abundances of NH_3 , H_2S , and H_2O on both planets are broadly consistent with expectations based on previous work by others [e.g. 7, 8], and highlight the compositional differences between gas- and ice-giant planets. On Saturn, the ground-based microwave observations have the potential to sound below the water cloud, constraining both the deep water abundance and exploring for the first time pressure-ionized regions of the atmosphere. This will require careful corrections due to background astronomical sources, and probably additional observations building on knowledge gained by the current attempts. We note that the shortest wavelength (~ 1 cm) Saturn data are not well matched by our models. We are currently assessing if these measurements might be in error or if there is temporal variability at these wavelengths.

For Uranus, planetary formation models [9 and references therein] indicate the bulk abundances of NH_3 and H_2S should be $>50\times$ solar, consistent with the measured bulk abundance of CH_4 . Also, solar abundances suggest there should be more NH_3 than H_2S . In the deep troposphere of Uranus, however, we find more H_2S than NH_3 and both are near or depleted from solar values. Atmospheric dynamics and the high-pressure liquid water ocean postulated to exist within ice giant planets may be responsible for depleting these species.

5. Conclusions

The composition, chemistry, and interior structure of the gas giant planet Saturn are very different from those of the ice giant Uranus.

Microwave observations can be used to probe these atmospheres from pressures of 1 to tens of thousands of bars.

Currently unknown chemical or dynamical processes are modifying the abundances of condensable species in the observable atmosphere of Uranus.

Acknowledgements

We thank the eVLA, IRTF, GMRT, LOFAR, and CSO observatories and staff for making these measurements possible. The work of MH and VA was carried out at the Jet Propulsion Laboratory, California Institute of Technology, under a contract with the National Aeronautics and Space Administration.

References

- [1] Courtin, R., Pandey-Pommier, M., Gautier, D., Zarka, P., and Hofstadter, M.: Metric observations of Saturn with the Giant Meterwave Radio Telescope, *BAAS* 46, p. 198, 2014.
- [2] Rodgers, C: *Inverse Methods for Atmospheric Sounding: Theory and Practice*, World Scientific, 2000.
- [3] Hofstadter, M., and Butler, B., Seasonal change in the deep atmosphere of Uranus, *Icarus* 165, pp. 168-180, 2003.
- [4] Devaraj, K., Steffes, P., Karpowicz, B., Reconciling the centimeter- and millimeter wavelength ammonia absorption spectra under jovian conditions, *Icarus* 212, pp. 224-235, 2011.
- [5] Karpowicz, B., and Steffes, P., Corrigendum to “In search of water vapor on Jupiter: Laboratory measurements of the microwave properties of water vapor under simulated jovian conditions”, *Icarus* 214, p. 783, 2011.
- [6] Bellotti, A., Steffes, P., and Chinsomboon, G., Laboratory measurements of the 5-20 cm wavelength opacity of ammonia, water vapor, and methane under simulated conditions for the deep jovian atmosphere, *Icarus* 280, pp. 255-267, 2016.
- [7] Gulkis, S., Janssen, M., and Olsen, E., Evidence for the depletion of ammonia in the Uranus atmosphere, *Icarus* 34, pp. 10-19, 1978.
- [8] de Pater, I., and Massie, S., Models of the millimeter-centimeter spectra of the giant planets, *Icarus* 62, pp. 143-171, 1985.
- [9] Atreya, S., Crida, A., Guillot, T., Lunine, J., Madhusudhan, N., and Mousis, O., The origin and evolution of Saturn, with Exoplanet perspective, in *Saturn in the 21st Century* (K. Baines, M. Flasar, N. Krupp, T. Stallard, eds), Cambridge University Press, 2018.

Spatial distribution of gaseous hydrogen cyanide on Neptune's stratosphere revealed by ALMA

Takahiro Iino (1), Sagawa Hideo (2) and Takashi Tsukagoshi (3)

(1) Tokyo University of Agriculture and Technology, Tokyo, Japan, (2) Kyoto Sangyo University, Kyoto, Japan, (3) National Astronomical Observatory of Japan, Tokyo, Japan

Abstract

We report the spatially resolved spectroscopic observation result of Neptune's stratospheric hydrogen cyanide ($J=4-3$) rotational transition at 354 GHz observed with Atacama Large Millimeter/submillimeter Array (ALMA) in April 2016. Spatial resolution and Neptune's angular diameter were 0.4 and 2.24 arcseconds, respectively. The molecular emission was clearly obtained over the Neptune's disk. Latitudinal variation of the integrated intensity that has the strongest peak at the equator was detected. Radiative transfer analysis indicates that the equatorial region has 50% higher column density value than that of 60 S region.

1. Introduction and imaging result

The presence of gaseous hydrogen cyanide (HCN) characterizes Neptune's stratospheric composition.

We analyzed an ALMA archived data of project ID 2015.1.01471.S (PI: R. Moreno), the same project as that of used in [1]. The data includes the HCN ($J=4-3$) rotational transition at 354.505 GHz. The observation was performed on 11:09 – 11:48, 30 April 2016 (UTC) using 41 12-m antennae.

The total bandwidth of the spectral window and the channel spacing were 1875 and 0.977 MHz, respectively. The total observing time of Neptune was 808.1 seconds. The apparent angular diameter of Neptune was 2.24 arcseconds.

The integrated-intensity map and the intensity plot measured at the same emission angle along the 0.95 arcseconds circular arc, which can exhibit the latitudinal intensity variation without the effect of different emission angles, are shown in Figure 1. Eastern and western hemisphere is plotted separately. An interesting feature was found for both hemispheres that the greatest intensity peak is locating at the equator. The lowest intensity values of both hemispheres locate at 70 S – 60 S.

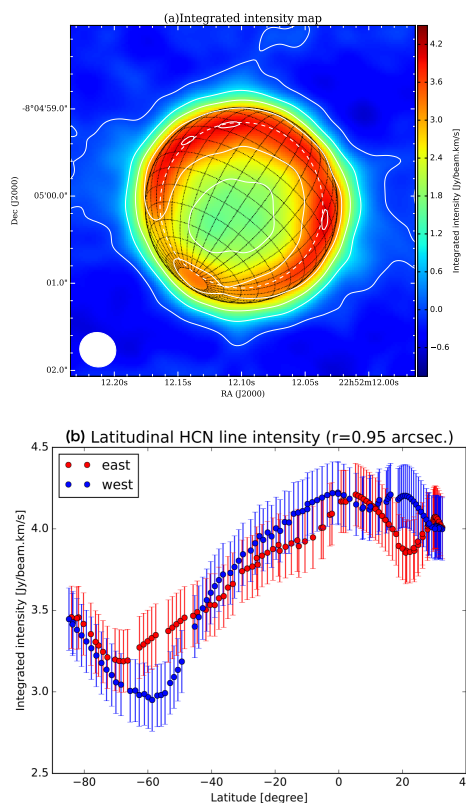


Figure 1: (top) An integrated intensity map of HCN ($J=4-3$) at 354.5 GHz obtained by ALMA. (bottom) Latitudinal variation of HCN integrated intensity for eastern and western hemispheres.

2. Radiative transfer analysis result

The HCN abundance was estimated by searching the best-fit spectrum through radiative transfer calculations. A modeled spatial resolution was 0.175 arc-seconds. Figure 2 presents an HCN column density map and a graph summarizing the latitudinal variation. The intensity distribution indicates increased levels of HCN over the equator, such that the equatorial HCN column density is $\sim 50\%$ higher than that in the 60 S region. The calculated disk-averaged column density, mixing ratio and p_0 values were $3.6 \pm 0.6 \times 10^{14}$ molecules cm^{-2} , $0.75^{+0.12}_{-0.13}$ ppb and $1.7^{+0.3}_{-0.4}$ mbar, respectively.

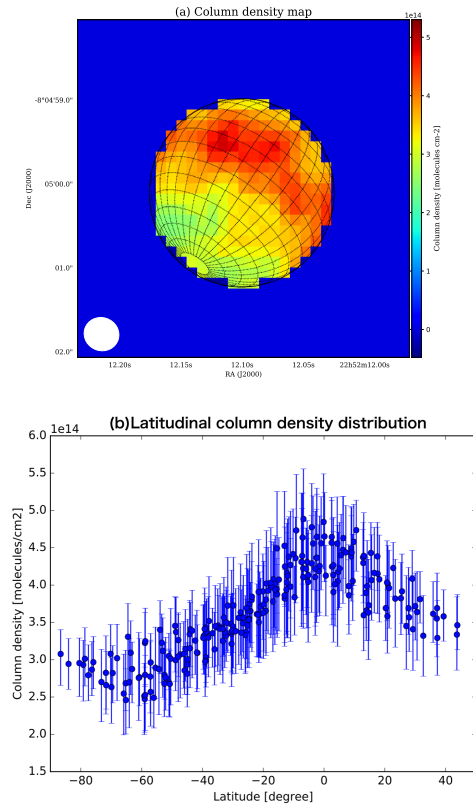


Figure 2: Spatial(top) and latitudinal(bottom) distribution of HCN column density.

3. Summary and Implications

We derived that Neptune's HCN shows non-uniform distribution in the stratosphere. A newly discovered HCN spatial distribution peak shows coincidence with where the downward motion was suggested by mid-IR and cm observations [2]. This coincidence could support a hypothesis that HCN is produced in the stratosphere and transported downwardly on the equator. In addition, a temporal decrease of the stratospheric temperature possibly decreases the HCN abundance.

Acknowledgements

This paper makes use of the following ALMA data: ADS/JAO.ALMA#2015.1.01471.S. ALMA is a partnership of ESO (representing its member states), NSF (USA) and NINS (Japan), together with NRC (Canada), MOST and ASIAA (Taiwan), and KASI (Republic of Korea), in cooperation with the Republic of Chile. The Joint ALMA Observatory is operated by ESO, AUI/NRAO and NAOJ. This work was financially supported by a JSPS Kakenhi grant (17K14420, TI) and an Astrobiology Center Program of National Institutes of Natural Sciences (NINS) grant.

References

- [1] Moreno, R., et al., (2017), Detection of CS in Neptune's atmosphere from ALMA observations. *A&A*, 608, L5. [2] de Pater, I., et al., (2014). Neptune's global circulation deduced from multi-wavelength observations. *Icarus*, 237, 211–238.

Forward and inverse kinetic energy cascades in Jupiter's turbulent weather layer

R. M. B. Young (1,2) and P. L. Read (1)

(1) Atmospheric, Oceanic and Planetary Physics, Department of Physics, University of Oxford, UK, (2) Laboratoire de Météorologie Dynamique (LMD/IPSL), Sorbonne Université, Centre National de la Recherche Scientifique, École Polytechnique, École Normale Supérieure, Paris, France (ryoung@lmd.jussieu.fr)

Abstract

Jupiter's atmosphere has often been compared with a classical quasi-2D, geostrophically turbulent fluid, with kinetic energy transferred upscale, and zonal jets emerging due to the planet's curvature. Using 2D wind fields obtained from Cassini cloud images taken during the December 2000 fly-by, we have measured the direction of Jupiter's kinetic energy cascade throughout the range of observed length scales, using structure functions and spectral fluxes as complementary approaches [5]. These confirm the upscale kinetic energy transfer from eddies on scales ≥ 3000 km up to the zonal jet scale, with $\sim 90\%$ of the energy transferred into the jets, and downscale transfer of enstrophy from all scales. At scales ≤ 3000 km or so, however, kinetic energy is transferred downscale, indicating a source at scales 2000–3000 km, comparable with the internal Rossby deformation radius. This suggests an important role for baroclinic instability in energising Jupiter's turbulent atmosphere.

1. Introduction

A distinctive characteristic of a turbulent flow is the nonlinear transfer of energy, vorticity and other flow properties between different scales of motion in processes known as cascades.

In homogeneous, isotropic 3D turbulence, nonlinear exchanges tend to cascade kinetic energy from large to small scales, where it is removed by viscous dissipation, leading to the Kolmogorov $-(5/3)$ law for the kinetic energy spectrum in the inertial range at intermediate scales. In a 2D or quasi-geostrophic system forced at scale L_f , the 'classical' picture suggests kinetic energy will generally cascade towards scales $\geq L_f$ while enstrophy cascades to scales $\leq L_f$, with energy spectra of slopes $-(5/3)$ and -3 respectively.

The prevailing view would anticipate that, given the strong dominance of planetary rotation on large-scale

motions on Jupiter, energy is likely to be mostly transferred upscale from the relatively small scales (dominated by convection or baroclinic instabilities) towards the scales of the zonal bands.

2. Cassini observations

Cassini flew by Jupiter in December 2000. We used horizontal winds calculated by two independent cloud tracking analyses of the CB2 near-infrared continuum band Imaging Science Subsystem images at closest approach. Datasets G14g [3] and C11 [2] contain gridded winds for almost four rotations over $\pm 50^\circ$ latitude and 360° longitude. Dataset G14s [6] contains scattered wind vectors from the 70 image pairs later stitched together to make dataset G14g.

3. Structure functions

The 3rd order structure function identifies the direction and kinetic energy propagation rate between different scales in a turbulent flow. It is calculated from velocity differences projected along (δu_L) or across (δu_T) a line separating pairs of points as a function of the separation distance r . For homogeneous isotropic turbulence, in 3D $\delta u_L^3 = -(4/5)\epsilon r$ where ϵ is the large-scale energy injection rate. In 2D turbulence, $\delta u_L^3 = +(3/2)Pr$ and $\delta u_L \delta u_T^2 = +(1/2)Pr$, where P is the energy input power due to a small-scale driving force [4]. In both 2D and 3D the 2nd order structure function $\delta u_L^2 \propto \epsilon^{2/3} r^{2/3}$.

Figure 1 shows a linear, positive dependence of the 3rd order structure functions on r for $3500 \text{ km} \leq r \leq 40\,000 \text{ km}$, implying an energy flux from small to large scales with $P \approx 1 \times 10^{-4} \text{ W kg}^{-1}$. Although not proportional to $r^{2/3}$ throughout, the second order structure function is consistent with the measured kinetic energy spectrum. At $r < 3500 \text{ km}$ the third-order structure functions are negative, implying downscale energy flux to small scales, contrasting the tra-

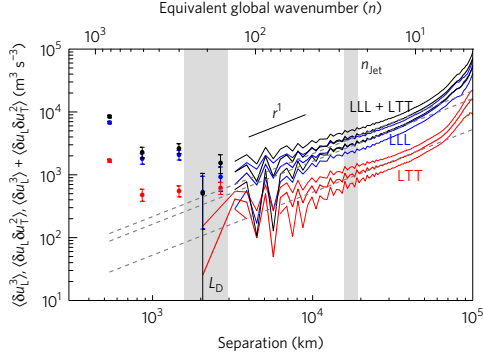


Figure 1: Third order structure functions, using dataset G14s. Grey bands show estimated deformation and jet scales. Dashed lines are linear fits. Dots are negative. Lines show means and 95% confidence intervals [5].

ditional picture of Jupiter’s atmospheric turbulence. A diverging energy flux implies that the turnaround scale contains a significant kinetic energy source for the flow.

4. Spectral fluxes

Positive spectral flux corresponds to energy transfer from large to small scales, and vice versa [1]. The kinetic energy flux, shown in Fig. 2, is negative and roughly flat between 4,000-15,000 km length scales, suggesting an inertial range with inverse cascade of power $\Pi_{E,\text{tot}}^{\text{up}} \approx (-5 \pm 2) \times 10^{-5} \text{ W kg}^{-1}$ from small scales to the jet scale. At scales ≤ 2000 km, the positive spectral flux corroborates our finding of downscale energy transfer at small scales in the structure functions, with $\Pi_{E,\text{tot}}^{\text{down}} \approx (+1.5 \pm 0.3) \times 10^{-5} \text{ W kg}^{-1}$.

There is a convergence of kinetic energy at the jet scale. This comes from larger scales (up to around 40,000 km) down to the jet scale and from smaller scales (down to around 2,500 km) up to the jet scale. All datasets show that the primary eddy to zonal flow energy conversion occurs at or near the jet scale. There is also remarkable agreement on the length scale at which the switch from upscale to downscale flux occurs. The agreement between this and a typical deformation radius in midlatitudes is striking.

5. Summary and Conclusions

The picture that emerges is a turbulent atmosphere energised by processes that generate kinetic energy

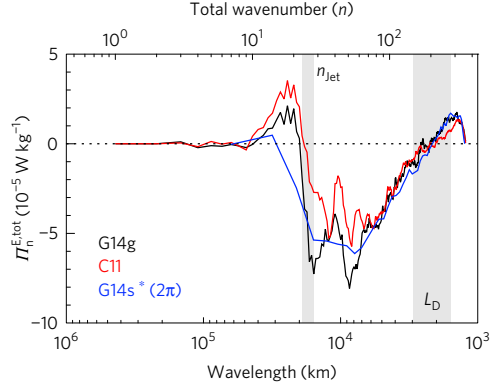


Figure 2: Kinetic energy spectral flux in Jupiter’s atmosphere, using all three datasets [5].

around the deformation scale, which then diverges upscale to the jet scale and downscale to small scales. This suggests an important role is played by baroclinic instability. The reversal of the energy cascade around the deformation scale suggests dynamical processes more like those in the Earth’s oceans than in its atmosphere. However, the flat part of the kinetic energy spectrum is quite non-terrestrial, and so Jupiter’s turbulence may not represent a ‘classical’ inertial range.

Acknowledgements

Support for RMBY was provided by UK STFC Grant ST/K00106X/1. This work was supported in part by the US National Science Foundation under Grant No. NSF PHY11-25915.

References

- [1] Burgess, B. H., Erler, A. R., and Shepherd, T. G., JAS, 70, 669–687, 2013.
- [2] Choi, D. S. and Showman, A. P., Icarus, 216, 597–609, 2011.
- [3] Galperin, B. et al., Icarus, 229, 295–320, 2014.
- [4] Lindborg, E., JFM, 388, 259–288, 1999.
- [5] Young, R. M. B. and Read, P. L., Nature Phys., 13, 1135–1140, 2017.
- [6] Young, R. M. B. et al., Oxford University Research Archive, 10.5287/bodleian:D5oVPJVRv, 2017.

Survey of lion roar emissions observed in Saturn's magnetosheath by Cassini

David Píša (1), A. H. Sulaiman (2), O. Santolík (1,3), G. B. Hospodarsky (2), W. S. Kurth (2), D. A. Gurnett (2)

(1) Department of Space Physics, Institute of Atmospheric Physics CAS, Prague, Czechia (2) Department of Physics and Astronomy, University of Iowa, Iowa City, U.S. (3) Faculty of Mathematics and Physics, Charles University, Prague, Czechia

Abstract

Whistler-mode waves known as lion roars have been observed by many missions inside the terrestrial magnetosheath. Recently, we have reported the evidence of such emissions in Saturn's magnetosheath [1]. In this study, we present a survey of these intense waves observed inside Saturn's magnetosheath by the Cassini spacecraft between years 2004 and 2011. We have identified all available time intervals of the intense lion roar emissions in the low-band (up to 50 Hz) RPWS/WFR spectrogram. The emissions were observed across the day-side magnetosheath. The emissions were narrow-banded with a peak frequency up to the lower-band cutoff (~ 30 Hz), well below the local electron cyclotron frequency (100–1000 Hz). Using the SVD method of the magnetic spectral matrices, we show that the waves are right hand circularly polarized and propagate at small wave normal angles (~ 5 degrees) with respect to the ambient magnetic field.

1. Introduction

A magnetosheath is a transient region between the solar wind and planetary magnetosphere. Inside the terrestrial magnetosheath, electromagnetic emissions, also known as lion roars, are often observed at frequencies 100–1000 Hz ($0.1\text{--}0.5 f_{ce}$, where f_{ce} is the local electron gyrofrequency). They are right-hand circularly polarized waves propagating at small wave normal angles ($< 15^\circ$) to the ambient magnetic field (see in Fig. 1).

The solar wind conditions at Saturn result in a magnetosheath that has different properties compared to Earth [2]. The plasma pressure varies between 6 and 30 pPa, the plasma density between 0.05 and 0.25 cm^{-3} , the plasma temperature between 210 and 370 eV, and plasma flow speed between 170 and 240 km s^{-1} . In the dawn region of Saturn's magnetosphere the average direction of plasma flow projected onto the ecliptic plane and measured counterclockwise

from the sunward direction has an angle in the range of $175\text{--}205$ degrees. The magnitude of the magnetic field is typically $0.6\text{--}1.6 \text{ nT}$ and results in a magnetic pressure of $0.2\text{--}1.1 \text{ pPa}$. The plasma β is in the range of $10\text{--}100$.

2. Data

The waveform receiver (WFR), a part of the Radio and Plasma Wave Science (RPWS) instrument, collects simultaneous waveforms from up to five sensors in a frequency range of either $1\text{--}26 \text{ Hz}$ (lower band) or $3 \text{ Hz--}2.5 \text{ kHz}$ (upper band). The waveforms are sampled at a frequency of 100 Hz with 12 bit resolution. The WFR snapshot with a length of 20.48 s is available every 24 s . During the analyzed time period the WFR receiver was measuring E_x and E_w signals from the electric antennas, and B_x , B_y , and B_z signals from the search coil instrument. An ambient magnetic field was obtained from the triaxial fluxgate magnetometer which is a part of the magnetometer (MAG) instrument. For the purpose of this study we used the list of time intervals inside the magnetosheath as identified in [2].

3. Summary and Conclusions

The lion roar emissions were observed across the day-side magnetosheath between magnetic local times from 0730 to 1600. The emissions were narrow-banded with a typical frequency at $0.16 f_{ce}$ (Fig. 2a). Using the singular value decomposition (SVD) method of the magnetic spectral matrices ([3], adapted for Cassini [4]), we show that the waves are right hand circularly polarized (Fig. 2b) and propagate at the typical wave normal angles of 5 degrees (Fig. 2c) with respect to the ambient magnetic field. Poynting flux directions (Fig. 2d) indicate that waves propagate parallel and anti-parallel to the ambient magnetic field lines.

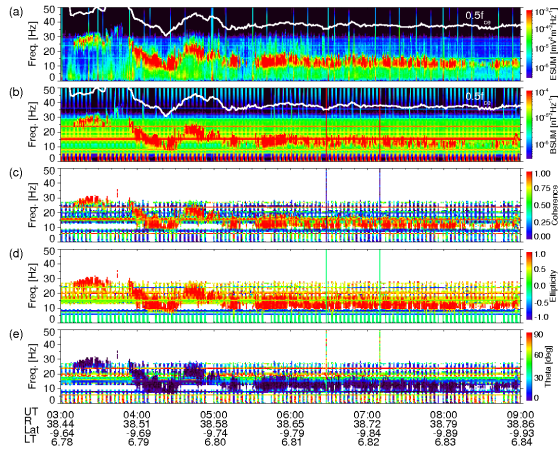


Figure 1: Cassini RPWS/WFR lower band data measured on 3 July 2005 as presented in [1]. (a and b) Sum of the power spectral densities of electric and magnetic field, respectively. The white line shows one half of the local electron gyrofrequency, f_{ce} . (c) Coherence in the polarization plane using the SVD method of the magnetic spectral matrices. (d) Ellipticity of the wave polarization combined with the sense of polarization, +1 for right-hand and -1 for the left-hand circularly polarized waves. (e) Polar angle of a wave vector, 0° for waves propagating parallel to the ambient magnetic field and 90° for transverse wave propagation.

We show the first long-term study of lion roar emissions outside the terrestrial environment. Our observations suggest that lion roars are a solar-system-wide phenomenon and capable of existing in a broad range of parameter space. This also includes 1 order of magnitude difference in frequencies. We anticipate our result to provide insight into such emissions in a vastly different parameter regime characterized by a higher plasma beta compared to Earth.

Acknowledgements

The authors are grateful to Nick Sergis for his list of Cassini’s magnetosheath visits. The authors also thank the CASSINI/MAG team for their support and for access to magnetometer data. The work has been supported by NASA through contract 1415150 with the Jet Propulsion Laboratory, from grant 16-6050Y of the Grant Agency of Czech Republic, from the MSM grant LTAUSA17070, and from the Praemium Academiae award.

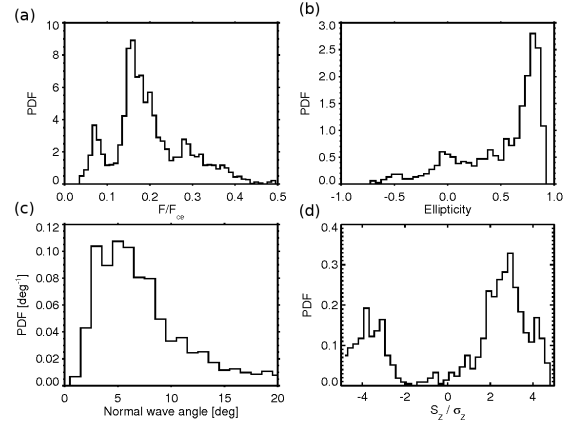


Figure 2: (a) Distribution of normalized frequencies for the most intense spectral peak of the sum of electric components. (b) Distribution of the ellipticity of wave polarization with the polarization sense. (c) Distribution of normal wave angles. (d) Distribution of the normalized Poynting flux component along the magnetic field with the level of confidence, positive values indicate parallel propagation and negative values anti-parallel propagation.

References

- [1] Pšša, D., Sulaiman, A. H., Santolík, O., Hospodarsky, G. B., Kurth, W. S., & Gurnett, D. A. (2018). First observation of lion roar emission in Saturn’s magnetosheath. *Geophys. Res. Letters*, 45. <https://doi.org/10.1002/2017GL075919>
- [2] Sergis, N., Jackman, C. M., Masters, A., Krimigis, S. M., Thomsen, M. F., Hamilton, D. C., et al. (2013). Particle and magnetic field properties of the Saturnian magnetosheath: Presence and upstream escape of hot magnetospheric plasma. *J. Geophys. Res. Space Physics*, 118, 1620–1634. <https://doi.org/10.1002/jgra.50164>
- [3] Santolík, O., Parrot, M., & Lefeuvre, F. (2003). Singular value decomposition methods for wave propagation analysis. *Radio Science*, 38, 1010. <https://doi.org/10.1029/2000RS002523>
- [4] Santolík, O., Gurnett, D. A., Jones, G. H., et al. (2011). Intense plasma wave emissions associated with Saturn’s moon Rhea. *Geophys. Res. Letters*, 38, L19204. <https://doi.org/10.1029/2011GL049219>

Global Flows Of Energetic Ions In Jupiter's Equatorial Plane During The Galileo Era 1995-2003

Norbert Krupp (1), B. Palmaerts (2), E. Roussos (1), M. Fränz (1), F. Bagenal (3), R. Wilson (3), C. Paranicas (4), K. Khurana (5)

- (1) Max-Planck-Institut für Sonnensystemforschung, Justus-von-Liebig-Weg 3, 37077 Göttingen, Germany
(2) Laboratoire de Physique Atmosphérique et Planétaire, Space Sciences, Technologies and Astrophysics Research (STAR), Université de Liège, Liège, Belgium
(3) Laboratory for Atmospheric and Space Physics, University of Colorado, Boulder, USA
(4) The Johns Hopkins University Applied Physics Laboratory, Laurel, MD, USA
(5) IGPP, University of California Los Angeles, Los Angeles, CA, USA

Abstract

The largest entity in our solar system besides the heliosphere itself is the Jovian magnetosphere. Its dimensions with a diameter of about 10 times the diameter of the Sun and its extension of more than 5 AU in the magnetotail as well as their richness of plasma processes makes it a special place. Understanding the global configuration and the dynamics of that magnetosphere is key to all the other magnetospheres in our solar system and beyond. Jupiter and its magnetic environment could serve a template for all the "Hot Jupiters" in other the universe. Brice and Ioannidis (1970) was among the first who described the Jovian system as a fast-rotating magnetosphere, highly stretched due to the centrifugal force due to mass-loading of magnetic field lines fed by the internal source Io and partially Europa.

One of the most important parameters of the Jovian magnetosphere is the understanding of the global flow patterns of plasma and energetic particles in Jupiter's magnetosphere. Early measurements taken by the particle spectrometers onboard the Pioneer 10 (P10) and 11 (P11), Voyager 1 (V1) and 2 (V2), and the Ulysses (ULS) spacecraft confirmed the predicted existence of a rotating magnetodisc of charged particles concentrated in the equatorial plane inside the fast-rotating system. Those early flyby data could only provide a snapshot of the flow patterns along the spacecraft trajectories. (Kane et al. (1992); Sands and McNutt (1988); Carbary et al. (1981), Bagenal et al. (2017); Bodisch et al. (2017); Dougherty et al. (2017)). P10, V1 and V2 left the magnetosphere through the predawn to dawn sector of the magnetosphere while P11 traversed along the high latitude noon magnetosphere. ULS added new data sets from three different instruments in the predawn

sector and provided the first hint of flow measurements in the southern high latitude dusk magnetosphere. Kolesnikova and Cowley (2002); Desai and Simnett (2000); Laxton et al. (1997, 1999); Kane et al. (1999); Hawkins III et al. (1998); Hawkins III (1997); Cowley et al. (1996); Staines et al. (1993); Staines et al. (1996); Desai and Simnett (1996); Hawkins III et al. (1995a,b). The global flow pattern, however, could not be derived before the Galileo spacecraft reached the planet and orbited Jupiter for almost 8 years covering a whole range of distances and local times. Krupp et al. (2001) used the directional ion anisotropies of the energetic particle instrument EPD for protons, oxygen and sulfur to derive the first global flow pattern. In their study measurements from the first 10 Galileo orbits were used covering the predawn to midnight sector of the Jovian magnetosphere. The interpretation derived from those measurements revealed that corotation of charged particle is observed throughout the magnetotail at least out to 150 RJ. The flows show a significant dawn-dusk asymmetry where the flows are much higher at dawn compared to dusk at similar distances. Waldrop et al. (2015) used EPD data again and found essentially the same flow results as Krupp et al. (2001). Krupp et al. (2015) has used the same analysis technique as in Krupp et al. (2001) but for all Galileo orbits. Bagenal et al. (2016) reanalyzed all the low energy ion data of the plasma instrument PLS onboard Galileo.

The purpose of this paper is to combine Galileo PLS and EPD measurements to derive the final global flow pattern in Jupiter's equatorial plane. In addition, the azimuthal flow as a function of distance and local time is used to map the corotation breakdown region in Jupiter's magnetosphere and compare it with a mapping of auroral imaging results of the main oval and a magnetic field model.

Acknowledgements

The Galileo data used in this study are available online through NASA PDS.

The German contribution of the EPD Instrument was in part financed by the DLR (Deutsches Zentrum für Luft- und Raumfahrt e.V.) under contracts No. 50 QJ 90032, 50 ON 0201 and 50 OH 0801 as well as by the Max-Planck-Gesellschaft. The JHUAPL portion of this work was supported in part by a NASA contract NAS5-97271 under task 006.

We thank A. Lagg (MPS) for providing a very powerful software package to analyze the EPD data set. We are also very grateful to T. Choo (JHUAPL) for reducing the EPD data.

A very special thanks goes to D. Williams, the Principal Investigator of the EPD instrument who always supported all the EPD team members in doing the science they want to do. The authors would also like to thank E. Roelof (JHUAPL) for very fruitful discussions early in the mission where he discovered an error in the EPD data analysis. We acknowledge also his brilliant mathematical ideas in deriving and interpreting the particle anisotropies.

Finally, we would like to dedicate this paper to B. Wilken (MPS) who passed away 2001 and had the idea of major parts of the EPD instrument. Without his help the results of this fantastic instrument would have never been possible.

References

- Bagenal, F., R. J. Wilson, S. Siler, W. R. Paterson, and W. S. Kurth, Survey of Galileo plasma observations in Jupiter's plasma sheet, *Journal of Geophysical Research (Planets)*, 121, 871-894, doi:10.1002/2016JE005009, 2016.
- Bagenal, F., L. P. Dougherty, K. M. Bodisch, J. D. Richardson, and J. M. Belcher, Survey of Voyager plasma science ions at Jupiter: 1. Analysis method, *Journal of Geophysical Research (Space Physics)*, 122, 8241-8256, doi:10.1002/2016JA023797, 2017.
- Bodisch, K. M., L. P. Dougherty, and F. Bagenal, Survey of Voyager plasma science ions at Jupiter: 3. Protons and minor ions, *Journal of Geophysical Research (Space Physics)*, 122, 8277-8294, doi:10.1002/2017JA024148, 2017.
- Brice, N. M., and G. A. Ioannidis, The Magnetospheres of Jupiter and Earth, *Icarus*, 13, 173, doi:10.1016/0019-1035(70)90048-5, 1970.
- Carbary, J. F., S. M. Krimigis, E. P. Keath, G. Gloeckler, W. I. Axford, and T. P. Armstrong, Ion anisotropies in the outer Jovian magnetosphere, *J. Geophys. Res.*, 86, 8285, 1981.
- Cowley, S. W. H., A. Balogh, M. K. Dougherty, M. W. Dunlop, T. M. Edwards, R. J. Forsyth, R. J. Hynds, N. F. Laxton, and K. Staines, Plasma flow in the Jovian magnetosphere and related magnetic effects: Ulysses observations, *J. Geophys. Res.*, 101, 15,197-15,210, 1996.
- Desai, M. I., and G. M. Simnett, Solar wind-driven flows in the Jovian magnetosphere, *J. Geophys. Res.*, 101, 13,115-13,136, 1996.
- Desai, M. I., and G. M. Simnett, Comment on: "Bulk Flows of hot Plasma in the Jovian Magnetosphere: A model of Anisotropic Fluxes of Energetic Ions" by S.E. Hawkins III, A.F. Cheng, and L.J. Lanzerotti, *J. Geophys. Res.*, 105 (A5), 10,771-10,778, 2000.
- Dougherty, L. P., K. M. Bodisch, and F. Bagenal, Survey of Voyager plasma science ions at Jupiter: 2. Heavy ions, *Journal of Geophysical Research*, 122, 8257-8276, doi:10.1002/2017JA024053, 2017.
- Hawkins III, S. E., Bulk flows of hot plasma in the Jovian magnetosphere, Ph.D. thesis, Johns Hopkins University, Baltimore, 1997.
- Hawkins III, S. E., A. F. Cheng, L. J. Lanzerotti, and C. G. MacLennan, Rotational anisotropy of the Jovian magnetosphere at high latitudes, *J. Geophys. Res.*, 100, 14,807-14,820, 1995a.
- Hawkins III, S. E., A. F. Cheng, L. J. Lanzerotti, and C. G. MacLennan, Corotation of Jupiter's three-dimensional magnetosphere, *Adv. Space Res.*, 16(4), 191-195, 1995b.
- Hawkins III, S. E., A. F. Cheng, and L. J. Lanzerotti, Bulk flow of hot plasma in the Jovian magnetosphere: A model of anisotropic fluxes of energetic ions, *J. Geophys. Res.*, 103 (E9), 20,031-20,054, 1998.
- Kane, M., B. H. Mauk, E. P. Keath, and S. M. Krimigis, A convected kappa-distribution model for

- hot ions in the Jovian magnetodisc, *Geophys. Res. Lett.*, 19, 1435-1438, 1992.
- Kane, M., D. J. Williams, B. H. Mauk, R. W. McEntire, and E. C. Roelof, Galileo energetic particles detector measurements of hot ions in the neutral sheet region of Jupiter's magnetodisc, *Geophys. Res. Lett.*, 26, 5-8, doi:10.1029/1998GL900267, 1999.
- Kolesnikova, E., and S. W. H. Cowley, The effect of instrument limitations on the derivation of plasma flows from energetic ion anisotropies, with an application to Ulysses observations at Jupiter, *Planet. Space Sci.*, 50, 193-215, 2002.
- Krupp, N., A. Lagg, S. Livi, B. Wilken, J. Woch, E. C. Roelof, and D. J. Williams, Global flows of energetic ions in Jupiter's equatorial plane: First order approximation, *J. Geophys. Res.*, 106, 26,017-26,032, doi:10.1029/2000JA900138, 2001.
- Krupp, N., J. Woch, A. Lagg, E. Roelof, D. Williams, S. Livi, and B. Wilken, Local time asymmetry of energetic ion anisotropies in the Jovian magnetosphere, *Planet. Space Sci.*, 49, 283-289, 2001.
- Krupp, N., E. Kronberg, and A. Radioti, Jupiter's Magnetotail, in *Magnetotails in the Solar System*, Washington DC American Geophysical Union Geophysical Monograph Series, vol. 207, edited by A. Keiling, C. M. Jackman, and P. A. Delamere, pp. 85-98, doi:10.1002/9781118842324.ch5, 2015.
- Laxton, N. F., A. Balogh, M. W. Dunlop, R. J. Forsyth, R. J. Hynds, K. Staines, and S. W. H. Cowley, Gradients and flows in Jupiter's magnetosphere determined from the anisotropies of approx.-1 MeV protons, *Adv. Space Res.*, 20, 221-224, 1997.
- Laxton, N. F., A. Balogh, S. W. H. Cowley, M. W. Dunlop, R. J. Hynds, D. J. McComas, and J. L. Phillips, Ulysses observations of field-perpendicular plasma flows in the Jovian magnetosphere: comparison of ExB velocity vectors derived from energetic ion and thermal electron data, *Planet. Space Sci.*, 47, 205-224, doi:10.1016/S0032-0633(98)00084-1, 1999.
- Sands, M. R., and R. L. McNutt, jr., Plasma bulk flow in Jupiter's dayside middle magnetosphere, *J. Geophys. Res.*, 93, 8502-8518, 1988.
- Staines, K., A. Balogh, S. W. H. Cowley, T. M. Edwards, R. J. Forsyth, and R. J. Hynds, Ulysses observations of noncorotational flows in the outer dayside Jovian magnetosphere, *Planet. Space Sci.*, 41, 931-946, doi: 10.1016/0032-0633(93)90098-M, 1993.
- Staines, K., A. Balogh, S. W. H. Cowley, T. M. Edwards, R. J. Forsyth, R. J. Hynds, and N. F. Laxton, An overview of the anisotropy telescope observations of MeV ions during the Ulysses Jupiter encounter, *Planet. Space Sci.*, 44 (4), 341-369, 1996.
- Waldrop, L. S., E. C. Roelof, and T. A. Fritz, Three-dimensional convective flows of energetic ions in Jupiter's equatorial magnetosphere, *Journal of Geophysical Research (Space Physics)*, 120, 10, doi:10.1002/2015JA021103, 2015.

Seasonal variations in Titan's stratosphere polar regions addressed with a Global Climate Model

Jan Vatat d'Ollone (1), Sébastien Lebonnois (1) and Jérémie Buralat (2)

(1) Sorbonne Université, École normale supérieure, PSL Research University, École polytechnique, CNRS, Laboratoire de Météorologie Dynamique / IPSL, Box 99, 4 place Jussieu, F-75005 Paris, France, (2) GSMA, UMR 7331, BP1039, Université de Reims Champagne-Ardenne, 51687 REIMS cedex, France (jan.vatat-dollone@lmd.jussieu.fr)

Abstract

In this study we present results concerning seasonal effects in Titan's stratosphere, modeled with the latest version of the IPSL Global Climate Model, and we compare them to Cassini's observations. Focus is put on the thermal structure on the polar night and especially the destabilization in low stratosphere observed with radio-occultations [4] and now reproduced closer to the observations in the simulations - without any latitudinal variation of composition neither radiative coupling with haze - even though a delay in the occurrence is noticed. This delay is also observed in terms of enrichment of trace compounds above winter pole, but the improvements brought to thermal structure and coupling with photochemical module lead to a better representation of the seasonal variations of minor species.

1. Introduction and Background

Observations of Saturn's moon Titan through exceptional longevity of Cassini's overall mission allowed to map stratospheric thermal structure and composition over almost half a Titan's year. Former works on these observations revealed many seasonal variations [6] among which some features remained unexplained or partially understood, such as the mechanisms in place in the polar vortex, the evolution of the thermal structure at high latitudes and the impact of the strong observed enrichment in trace compounds in winter polar nights.

The latest works on the IPSL Titan's Global Climate Model (GCM) radiative transfer, now based on a flexible correlated-k method and up-to-date gases spectroscopic data [5], lead to a correct modeling of the temperature profiles in the middle atmosphere. It also induced a better representation of the circulation which bring new results in this part of the atmosphere for simulations coupled with photochemical module.

Given this, it is now possible to tackle some scientific issues about seasonal variations of thermal structure and minor species mixing ratio in polar regions.

2 Thermal structure above winter pole

As the former microphysical model used in the reference version of the GCM [3] needed to be switched off so far in this new version, we present in a first time results concerning simulations without radiative retroaction of haze variations, with the same mean vertical profile of haze extinction being used at all latitudes and seasons.

Special interest is bear on the destabilization of lower polar winter stratosphere, such as observed by Cassini radio-occultations [4], now reproduced in simulations as shown in Figure 1.

Nevertheless we notice that in these simulations this destabilization appear in the autumn and early winter whereas it has been observed later, up to the following equinox, by Cassini.

Upper in the stratosphere the thermal profiles are too warm above winter pole as we for now lack the strong infrared cooling caused by accumulation of haze in this area.

3 Seasonal variations of trace compounds

We will also present the coupling of this new version of the GCM with our photochemical solver [2], extended up to 1300 km, and the consequences of the improved thermal structure and mixing in the middle atmosphere on the seasonal distribution of trace compounds. In light of the results of coupled simulations, we will discuss questions raised by observa-

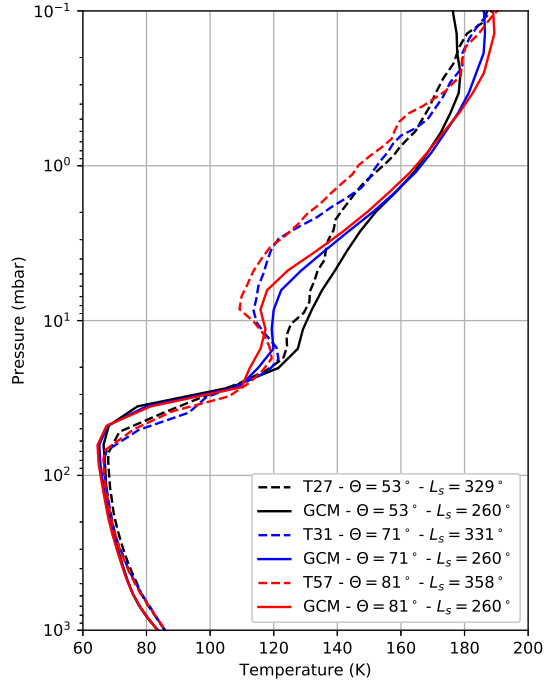


Figure 1: Thermal profiles simulated in the winter hemisphere compared to Cassini radio-occultations [4]. The destabilization in low stratosphere at high latitudes - although it happens too early in our simulations - is obtained without adding any radiative retro-action of haze or chemical compounds.

tions, such as the delay between circulation reversal at the equinox and reversal of the chemical enrichment as well as the strength of this enrichment for various species.

4. Conclusions and Perspectives

In this study we show that interesting results about polar regions thermal structure and composition can be obtained and discussed with simulations without radiative coupling of haze or chemical compounds. As adding these to the model would open broader perspectives, we will discuss the challenges addressed by re-coupling a new microphysical moments scheme developed recently [1] – in the perspective of having a fully interactive microphysical-chemical-dynamical coupled model – and first results of this work will be presented.

References

- [1] Burgalat, J. and Rannou, P.: Brownian coagulation of a bi-modal distribution of both spherical and fractal aerosols, *Journal of Aerosol Science*, 105, pp. 151-165, 2016.
- [2] Cresspin, A. et al: Diagnostics of Titan's stratospheric dynamics using Cassini/CIRS data and the 2-dimensional IPSL circulation model, *Icarus*, 197, pp. 556-571, 2008.
- [3] Lebonnois, S. et al: Titan Global Climate Model: new 3-dimensional version of the IPSL Titan GCM, *Icarus*, 218, pp. 707-722, 2012.
- [4] Schinder, P. J. et al: The structure of Titan's atmosphere from Cassini radio occultations: Occultations from the Prime and Equinox missions, *Icarus*, 221, pp. 1020-1031, 2012.
- [5] Vatat d'Ollone, J. et al: Modelling of Titan's middle atmosphere with the IPSL climate model, *EGU General Assembly*, Vienna, Austria, 2017.
- [6] Vinatier, S. et al: Seasonal variations in Titan's middle atmosphere during the northern spring derived from Cassini/CIRS observations, *Icarus*, 250, pp. 95-115, 2015.

Modeling atmospheric dynamics in Jupiter's troposphere

Alexandre Boissinot, Aymeric Spiga, Sandrine Guerlet and Simon Cabanes

Laboratoire de Météorologie Dynamique, Sorbonne Université, Paris, France (alexandre.boissinot@lmd.jussieu.fr)

1. Introduction

1.1. Observational background

Jupiter's tropospheric dynamics is characterised by the presence of alternately prograde and retrograde jet streams whose speeds are included between 10 and 150 m s⁻¹ and which delimit zones and belts, where wind shear is respectively anticyclonic and cyclonic [10]. The equatorial jet is superrotating with a velocity equal to 100 m s⁻¹. Some large vortices like the Great Red Spot (GRS) and the White Ovals can be observed (from 10³ km large to 10⁴ by 2 10⁴ km for the GRS), as well as convective storms and lightnings, particularly studied by Galileo [8] and Cassini [3] missions. These storms are typically few thousands kilometers large and occur almost exclusively in belts but since the Juno mission reached Jupiter, we can see some features that look like small (100 km large) convective clouds in zones. The Juno mission has especially revealed Jupiter turbulent poles and polar clusters of cyclones [1].

1.2. Modeling context

To model solar system gas giant atmosphere, there are two kind of models : deep models (for example [5]) and shallow models. Both imply an inverse cascade of energy from small-scale eddies to large-scale jets due to the fast rotation rate of these planets. The difference is the perturbation source: magnetohydrodynamics effects at great depth in the first case, baroclinic instabilities or convection in the second one. We place ourselves in the second case and try to reproduce jovian tropospheric main features.

2. Model

For that, we use a gas giant General Circulation Model (GCM) which contains a dynamical core and several physical parametrizations. The dynamical core DY-NAMICO solves atmospheric primitive equations under the shallow water and hydrostatic assumptions on an icosahedral grid [2] to ensure good energy and momentum conservation as good scalability properties

for massively parallel computing. The main physical parametrization is the radiative model adapted from Saturn to Jupiter [4], which uses the k-distribution method. A Rayleigh friction is added at the base of the model to parametrize a deeper drag due to magnetohydrodynamics effects [9]. Eventually, to model the troposphere, we need to include the stratosphere in our GCM in order to model correctly the tropopause and avoid side effects.

3. Results and possibilities

In high resolution simulations (0.5 degree resolution in longitude and latitude), we can see about ten jets which are alternately prograde and retrograde (*cf.* figures 1 and 2). Their speed has the good order of magnitude in absolute value but the equator show a subrotation instead of a superrotation. But above all they are too broad and too few and their migration toward high latitudes, which takes place during the first years of the simulation, reduces this number to height. We investigate these issues and will discuss about the results during the conference.

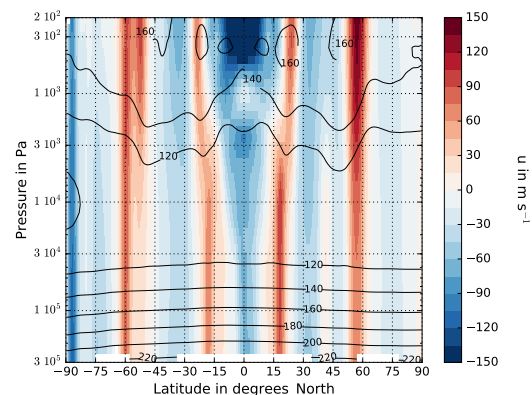


Figure 1: Zonal mean zonal wind (in m s⁻¹) in function of pressure and latitude after 4 simulated jovian years with temperature contours (in K).

One possibility to explain the differences between simulations and observations is the absence of convection parametrization. Indeed, convective activity is supposed to be one of the large-scale circulation energy sources and able to modify jets width and speed [7]. Therefore we are replacing the simple convective adjustment by a moist convection parametrization. We chose the thermal plume model originally developed in LMD [6] to model Earth boundary-layer convection and adapted to moist convection ([11], [12]). The choice relevance and the effects of the parametrization on the simulated large-scale circulation will be discussed during the conference.

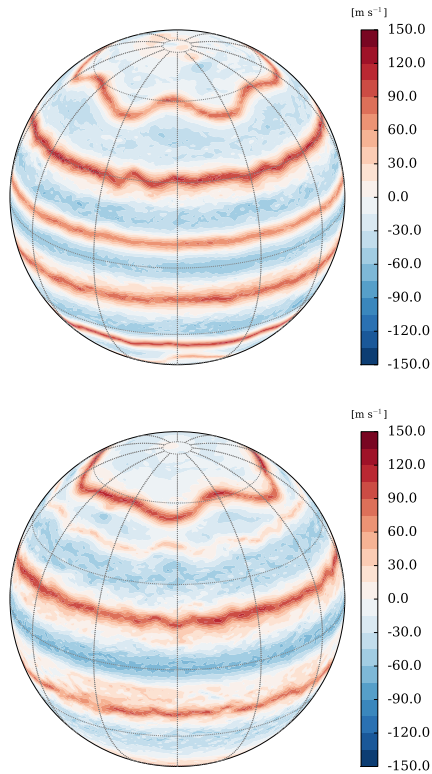


Figure 2: Zonal wind speed (in m/s) at the 1-bar pressure level after 1 (top) and 4 (bottom) simulated jovian years.

References

- [1] Adriani, A., Mura, A. *et al.*: Clusters of cyclones encircling Jupiter's poles, *Nature*, Vol. 555, pp. 216-219, 2018.
- [2] Dubos, T., Dubey, S. *et al.*: DYNAMICO-1.0, an icosahedral hydrostatic dynamical core designed for consistency and versatility, *Geoscientific Model Development*, Vol. 8, pp. 3131–3150, 2015.
- [3] Dyudina, U., Del Genio, A. *et al.*: Lightning on Jupiter observed in the $H\alpha$ line by the Cassini imaging science subsystem, *Icarus*, Vol. 172, pp. 24-36, 2004.
- [4] Guerlet, S. and Spiga, A.: Radiative and dynamical modeling of Jupiter's atmosphere, *EGU General Assembly Conference*, 17-22 April 2016, Vienna, Austria, 2016.
- [5] Heimpel, M. and Aurnou, J.: Turbulent convection in rapidly rotating spherical shells: A model for equatorial and high latitude jets on Jupiter and Saturn, *Icarus*, Vol. 187, pp. 540-557, 2007.
- [6] Hourdin, F., Couvreur, F. and Menut, L.: Parameterization of the Dry Convective Boundary Layer Based on a Mass Flux Representation of Thermals, *Journal of the Atmospheric Sciences*, Vol. 59, pp. 1105-1123, 2002.
- [7] Li, L., Ingersoll, A. and Huang, X.: Interaction of moist convection with zonal jets on Jupiter and Saturn, *Icarus*, Vol. 180, 113-123, 2006.
- [8] Little, B., Clifford, D. *et al.*: Galileo Images of Lightning on Jupiter, *Icarus*, Vol. 142, pp. 306-323, 1999.
- [9] Liu, J. and Schneider, T.: Mechanisms of Jet Formation on the Giant Planets, *Journal of the Atmospheric Sciences*, Vol. 67, pp. 3652-3672, 2010.
- [10] Porco, C., West, R. *et al.*: Cassini Imaging of Jupiter's Atmosphere, Satellites, and Rings, *Science*, Vol. 299, pp. 1541-1547, 2003.
- [11] Rio, C. and Hourdin, F.: A Thermal Plume Model for the Convective Boundary Layer: Representation of Cumulus Clouds, *Journal of the Atmospheric Sciences*, Vol. 65, pp. 407-425, 2008.
- [12] Rio, C., Hourdin, F., Couvreur, F. and Jam, A.: Resolved Versus Parametrized Boundary-Layer Plumes. Part II: Continuous Formulations of Mixing Rates for Mass-Flux Schemes, *Boundary-Layer Meteorology*, Vol. 135, pp. 469-483, 2010.

First Ion Insights during Titan's Ionosphere Relevant Gas Mixture EUV Irradiation

Jérémy Bourgalais, Ludovic Vettier, Sarah Tigrine, Guy Cernogora and Nathalie Carrasco

Université Versailles St-Quentin, Sorbonne Université, UPMC Univ. Paris 06, CNRS/INSU, LATMOS-IPSL, 11 boulevard d'Alembert, 78280 Guyancourt, France (jeremy.bourgalais@latmos.ipsl.fr)

Abstract

In Titan's ionosphere, the chemical growth in the atmosphere is believed to occur through the chemical coupling of radicals and reactive charged species but the complexity of the chemistry is far from being understood. Here we present a series of EUV Titan's atmosphere simulation experiments. We irradiated at 73.6nm different gas mixtures (N_2/CH_4 & He/CH_4) in a photochemical reactor. Our work is focused for the first time on photochemical ionic products.

1. Introduction

The arrival of the Cassini-Huygens spacecraft led to the discovery of an unexpected efficient organic chemistry, including very heavy ionic species [1,2] in the Titan's thermosphere. It showed that large condensable molecules are formed in the upper region of the moon where the flux of photons partly initiate chemical reactions. The photochemistry of CH_4 is one of the dominant chemical processes, but the large amount of N_2 is believed to significantly change the subsequent chemistry. As a matter of fact, the instruments onboard to the Cassini spacecraft showed that nitrogen participates in the chemistry and Titan's aerosols contain significant amounts of nitrogen [3,4]. In addition, Titan's atmosphere simulation experiments [5-7] have also demonstrated that the presence of nitrogen increases the molecular complexity. However, even if the chemical growth in the atmosphere is believed to occur through the chemical coupling of radicals and reactive charged species (ionic species and electrons) the complexity of the chemistry is far from being understood. Indeed, the current photochemical models [8] reasonably explain the formation of small carbon/nitrogen bearing molecules, but fail at giving accurate processes for the formation of heavy C and/or N-based species observed (>4 carbon and/or nitrogen atoms). It is mainly due to the complexity of reaction pathways and the limited set of available

data (branching ratios and coefficient rates) for chemical reactions.

2. Experimental Approach

Numerous laboratory studies investigated the gas phase products in the atmosphere of Titan through irradiation of N_2/CH_4 mixtures by using a variety of energy sources (e.g., laser induced plasma, electrical discharge, UV lamps or synchrotron). However, those sources, despite synchrotron beamline, allow to work only above 110nm. Indeed, it requires EUV wavelengths (<110 nm) in order to address the effect of photoionisation of nitrogen as it might plays a key role in the upper part of the atmosphere of Titan regarding the ionization cross section at these wavelengths and the abundance of the molecule. There is only one EUV synchrotron radiation study on N_2/CH_4 gas mixture [7,9,10]. They have shown that the presence of the dominant nitrogen species in the gas mixture (ca. 95%) enhances the formation of unsaturated hydrocarbons (e.g., benzene, toluene) at wavelength below 80nm. The production is believed to initially come from a dissociative charge-transfer reaction between N_2^+ and methane, leading to the formation of unsaturated complex hydrocarbons through production of $C_2H_5^+$ with subsequent dissociative recombination. However, they were not able to look at ions to validate this mechanism assumption.

Our work aims at corroborating the major role, highlighted by Imanaka *et al.*, played by the photoionization of nitrogen in the formation of complex organic molecules by monitoring simultaneously neutral and ion EUV photoproducts.

3. Results

Accordingly, here we present a series of EUV Titan's atmosphere simulation experiments. We irradiated at 73.6nm different gas mixtures (N_2/CH_4 & He/CH_4) in

the APSIS (Atmospheric Photochemistry Simulated by Synchrotron) reactor recently developed in the LATMOS laboratory [11]. The wavelength is obtained by using a surfatron-type discharge with a neon gas flow in the mbar pressure range coupled to the photochemical APSIS reactor. This experimental setup designed to carry research on planetary atmospheres allow *in situ* mass spectrometry analysis of the neutral and ionic species produced in the APSIS reactor.

The first experiment analysis for the photolysis of only methane seems to confirm the assumption of Imanaka *et al.* with CH_5^+ and C_2H_5^+ as the main ion species. However, in the case of a coupled N_2/CH_4 system, CH_3^+ is not the main contributor for the growth of the unsaturated species. The formation seems to be driven by nitrogen species such as N_2^+ , HCNH^+ and NH_4^+ . As shown in Figure 1 illustrating a mass spectrum of the positive ions detected in the photochemical reactor obtained from a N_2/CH_4 gas mixture irradiated 73.6nm. We also notice an efficient ion production up to m/z 150.

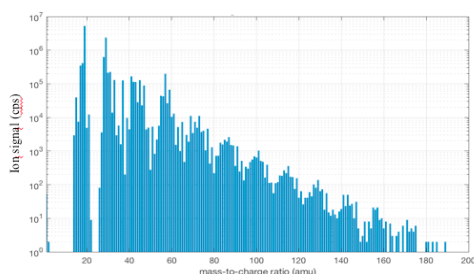


Figure 1: Positive ions mass spectrum obtained from a N_2/CH_4 gas mixture irradiated 73.6nm

This work constraints the detailed chemical mechanisms by bringing for the first time information about ionic and neutral species formed in nitrogen-dominated atmospheres by EUV irradiation. This work is important to reduce the sources of uncertainty and/or bias in the model predictions of Titan's ionosphere.

Acknowledgements

This research is supported by the ERC Starting Grant PRIMCHEM, grant agreement n°636829.

References

- [1] Coates, A. J., Crary, F. J., Lewis, G. R., Young, D. T., Waite, J. H., & Sittler, E. C. (2007). *Geophysical Research Letters*, 34(22).
- [2] Crary, F. J., Magee, B. A., Mandt, K., Waite Jr, J. H., Westlake, J., & Young, D. T. (2009). *Planetary and Space Science*, 57(14-15), 1847-1856.
- [3] Israël, G., Szopa, C., Raulin, F., Cabane, M., Niemann, H. B., Atreya, S. K., et al. (2005). *Nature*, 438(7069), 796.
- [4] Vuitton, V., Yelle, R. V., & McEwan, M. J. (2007). *Icarus*, 191(2), 722-742.
- [5] Sebree, J. A., Trainer, M. G., Loeffler, M. J., & Anderson, C. M. (2014). *Icarus*, 236, 146-152.
- [6] Trainer, M. G., Sebree, J. A., Yoon, Y. H., & Tolbert, M. A. (2013). *The Astrophysical Journal Letters*, 766(1), L4.
- [7] Imanaka, H., & Smith, M. A. (2009). *The Journal of Physical Chemistry A*, 113(42), 11187-11194.
- [8] Moses, J. I., Fouchet, T., Bézard, B., Gladstone, G. R., Lellouch, E., & Feuchtgruber, H. (2005). *Journal of Geophysical Research: Planets*, 110(E8).
- [9] Imanaka, H., & Smith, M. A. (2007). *Geophysical research letters*, 34(2).
- [10] Imanaka, H., & Smith, M. A. (2010). *Proceedings of the National Academy of Sciences*, 107(28), 12423-12428.
- [11] Tigrine, S., Carrasco, N., Vettier, L., & Cernogora, G. (2016). *Journal of Physics D: Applied Physics*, 49(39), 395202.

30 Years of H_3^+ Planetary Astronomy

Steve Miller

Department of Science and Technology Studies / Physics and Astronomy, University College London, Gower Street, London WC1E 6BT, United Kingdom (s.miller@ucl.ac.uk)

Abstract

On September 21, 1988, a team of French, Korean and Canadian astronomers made their way to the summit of Mauna Kea in Hawai'i to make use of the Canada-France-Hawai'i Telescope to observe the powerful aurorae of Jupiter. They were looking for infrared emission at 2.122 microns from the H_2 $v=1 \rightarrow 0$ S(1) quadrupole line, using the telescope's high-spectral resolution Fourier-transform spectrometer. That line was clearly observed.

But alongside the H_2 line was a slew of other, equally bright if not brighter lines, that could not be immediately identified. A worldwide collaboration – including the Molecular Physics Group at UCL – showed that the lines were from the H_3^+ molecular ion, the first time this fundamental species had been seen outside of the laboratory. This talk will outline the use that astronomers have made of H_3^+ emissions from Jupiter, Saturn and Uranus over the last 30 years, including:

1. Probing physical conditions in the upper atmospheres of these planets;
2. Exploring the dynamics of thermosphere-ionosphere-magnetosphere coupling;
3. Illuminating interactions between planetary magnetospheres and solar wind conditions the local space environment;
4. Helping us to understand measurements from ground-based observatories and space missions such as Galileo, Hubble, Cassini and JUNO.